Akademia Górniczo-Hutnicza im. Stanisława Staszica w Krakowie
WYDZIAŁ FIZYKI I INFORMATYKI STOSOWANEJ

KATEDRA ODDZIAŁYWAŃ I DETEKCJI CZĄSTEK

Praca dyplomowa

Measurement of the inclusive production of neutral meson K and neutral barion Lambda in proton-proton diffraction collisions at center-of-mass energy of 510 GeV in the STAR experiment at RHIC

Pomiar inkluzywnej produkcji neutralnego mezonu K oraz neutralnego barionu Lambda w dyfrakcyjnym oddziaływaniu proton-proton przy energii 510 GeV w układzie środka masy w eksperymencie STAR na akceleratorze RHIC.

Autor:	Adam Wątroba
Kierunek studiów:	Fizyka Techniczna
Opiekun pracy:	dr inż. Leszek Adamczyk

Kraków, 2024

Abstract

During proton-proton collisions, in small part of events, both protons survive and are scattered at very small angles, producing particles in the central rapidity region. This type of reaction (central diffraction) takes place by the exchange of two so called Pomerons, which in lowest order of QCD can be modelled as pairs of gluons. In the aforementioned process, central state with quantum numbers of a vacuum is produced, and the particles produced (or the products of their decays) can be measured. In this thesis my main focus is K^0 and Λ^0 measurement as a result of $p + p \to p + p + K^0(\Lambda^0) + X$ reaction at $\sqrt{s} = 510$ GeV. Such process can be measured by STAR experiment at RHIC. Roman Pots detectors will be used to measure scattered protons, and central state detector will be used to measure the remaining produced particles. The aim of this analysis is to obtain diffractive yields with respect to various kinematic variables, which can further be used to calculate cross sections for this reaction.

Contents

1 Introduction

1.1 Standard Model and K^0, Λ^0 particles

Current, most widely accepted theory predicting matter properties at the most basic level is called the Standard Model. It predicts various properties, such as three existing "flavours" of particles, or the way quarks interact by gluon exchange. Out of four fundamental forces in the universe - gravitational, electromagnetic, weak and strong interactions - the latter three are described in SM. Gravity is governed by General Relativity and at this level is not important to us.

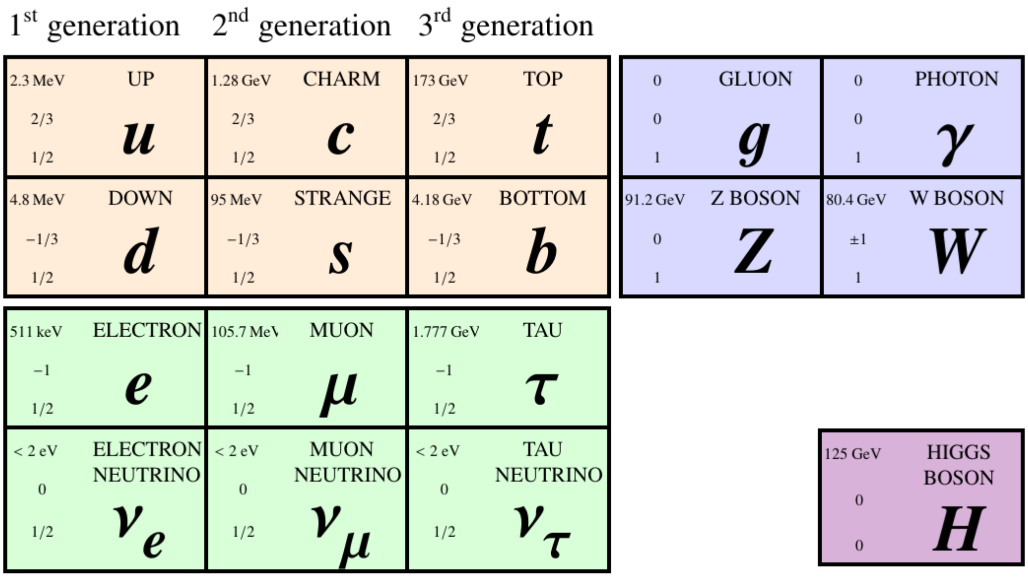

1st generation	2nd generation	3rd generation		
2.3 MeV 2/3 1/2 UP u	1.28 GeV 2/3 1/2 CHARM c	173 GeV 2/3 1/2 TOP t	0 0 1 GLUON g	0 0 1 PHOTON γ
4.8 MeV −1/3 1/2 DOWN d	95 MeV −1/3 1/2 STRANGE s	4.18 GeV −1/3 1/2 BOTTOM b	91.2 GeV 0 1 Z BOSON Z	80.4 GeV ±1 1 W BOSON W
511 keV −1 1/2 ELECTRON e	105.7 MeV −1 1/2 MUON μ	1.777 GeV −1 1/2 TAU τ		
< 2 eV 0 1/2 ELECTRON NEUTRINO ν_e	< 2 eV 0 1/2 MUON NEUTRINO ν_μ	< 2 eV 0 1/2 TAU NEUTRINO ν_τ		125 GeV 0 0 HIGGS BOSON H

Figure 1: Table of Standard Model, grouped by particle type: quarks - pink, leptons - green, gauge bosons - blue, Higgs boson - purple. Mass, charge, and spin are listed for each on the left. Data taken from [1]

In *pp* collisions, particle creation happens through strong interactions, which are carried by gluons. Gluons are massless, vector bosons of spin 1, and additionally have a property called "colour", which has three possible values ("red", "green", "blue"). Due conservation of quantum numbers, such as aforementioned colour, but also charge, spin etc. multiple gluons are being exchanged in these processes. Theory governing such behaviour is called Quantum Chromodynamics (QCD). One of the limitations occurring is so called colour confinement - due to strong interaction potential behaving differently than electromagnetic one, force acting upon quarks in further distance is almost constant, causing particle creation at longer distances in a process called hadronization. In these processes (due to their relatively small masses) the most abundant particles created are pions ($\pi^{\pm}, \pi^0$) and kaons ($K^{\pm}, K^0$), although heavier particles (like Λ^0 baryons) are also possible to produce.

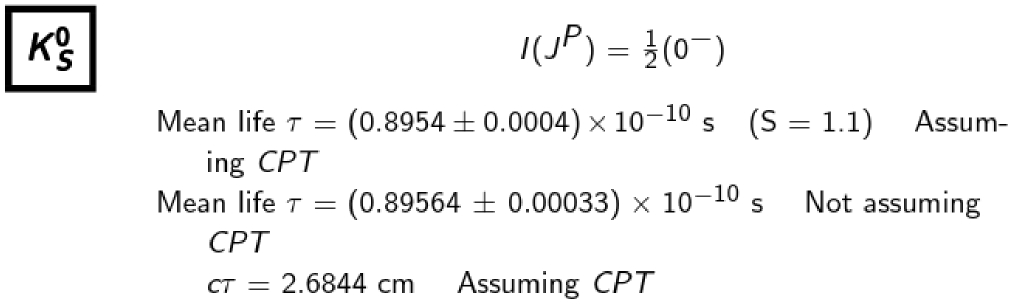

K_S^0

$I(J^P) = \frac{1}{2}(0^-)$

Mean life $\tau = (0.8954 \pm 0.0004) \times 10^{-10}$ s (S = 1.1) Assuming CPT

Mean life $\tau = (0.89564 \pm 0.00033) \times 10^{-10}$ s Not assuming CPT

$c\tau = 2.6844$ cm Assuming CPT

Figure 2: PDG entry of K_S^0 meson

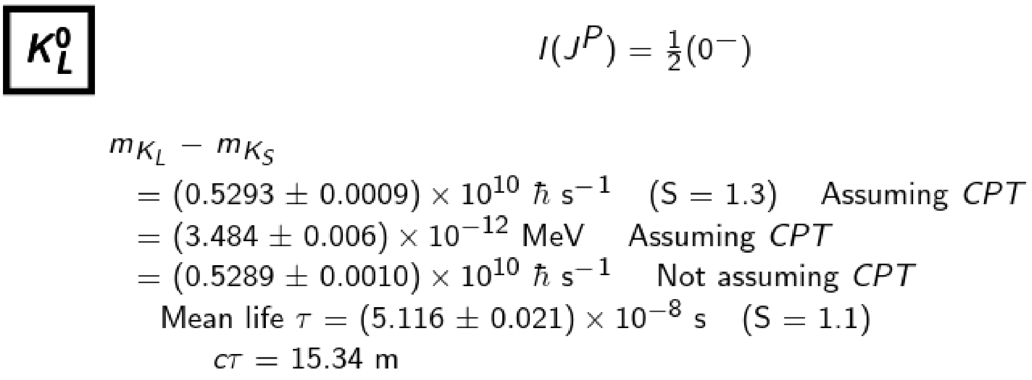

K_L^0

$I(J^P) = \frac{1}{2}(0^-)$

$m_{K_L} - m_{K_S}$

$= (0.5293 \pm 0.0009) \times 10^{10}\ \hbar\ s^{-1}$ (S = 1.3) Assuming CPT

$= (3.484 \pm 0.006) \times 10^{-12}$ MeV Assuming CPT

$= (0.5289 \pm 0.0010) \times 10^{10}\ \hbar\ s^{-1}$ Not assuming CPT

Mean life $\tau = (5.116 \pm 0.021) \times 10^{-8}$ s (S = 1.1)

$c\tau = 15.34$ m

Figure 3: PDG entry of K_L^0 meson

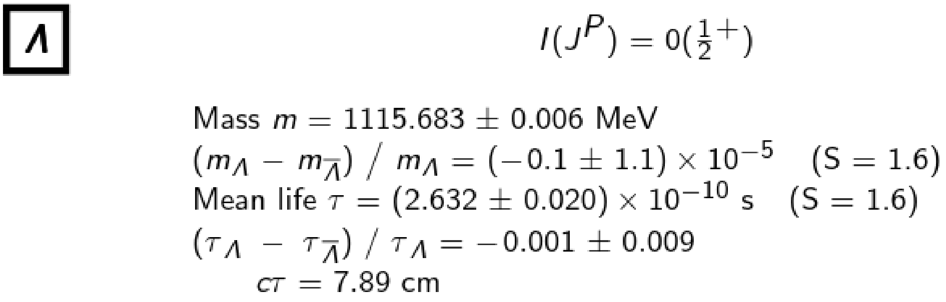

Λ

$I(J^P) = 0(\frac{1}{2}^+)$

Mass $m = 1115.683 \pm 0.006$ MeV

$(m_\Lambda - m_{\overline{\Lambda}}) / m_\Lambda = (-0.1 \pm 1.1) \times 10^{-5}$ (S = 1.6)

Mean life $\tau = (2.632 \pm 0.020) \times 10^{-10}$ s (S = 1.6)

$(\tau_\Lambda - \tau_{\overline{\Lambda}}) / \tau_\Lambda = -0.001 \pm 0.009$

$c\tau = 7.89$ cm

Figure 4: PDG entry of Λ^0 baryon

Due to neutral particle oscillations caused by weak decay not conserving flavours, K^0 meson actually exists in two eigenstates, K_S^0 and K_L^0, named because of respectively relatively short and long decay times (giving us decay length of 2.68 cm and 15.34 m, as seen on Figures 2 and 3, taken from Particle Data Group (PDG)[2]). Given probability of decay in range of detection and chance of products being only detectable, charged particles (69.20 % for $K_S^0 \to \pi^+\pi^-$ vs 67.59 % for $K_L^0 \to \pi^\pm l^\mp \nu_l$ per PDG entries on Figures 5 and 6), K_S^0 is a natural candidate for detection.
Neutral Lambda baryon (Λ^0) does not have such problems, and its main decay channel (63.9% for $\Lambda^0 \to p^+\pi^-$ per PDG entry on Figure 7), as well as similar decay length (7.89 cm) makes it possible to detect using similar cuts as were used for K_S^0.

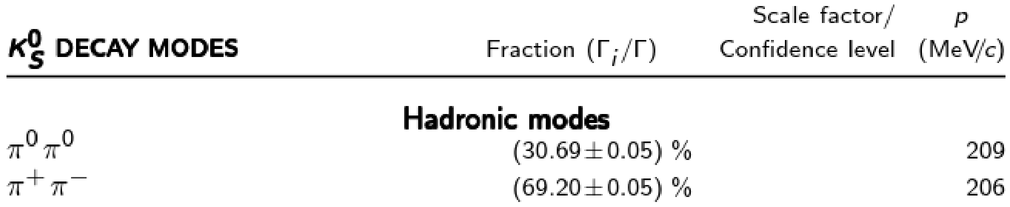

K_S^0 DECAY MODES	Fraction (Γ_i/Γ)	Scale factor/ Confidence level	p (MeV/c)
Hadronic modes			
$\pi^0\pi^0$	(30.69 ± 0.05) %		209
$\pi^+\pi^-$	(69.20 ± 0.05) %		206

Figure 5: Decay modes of of K_S^0 meson

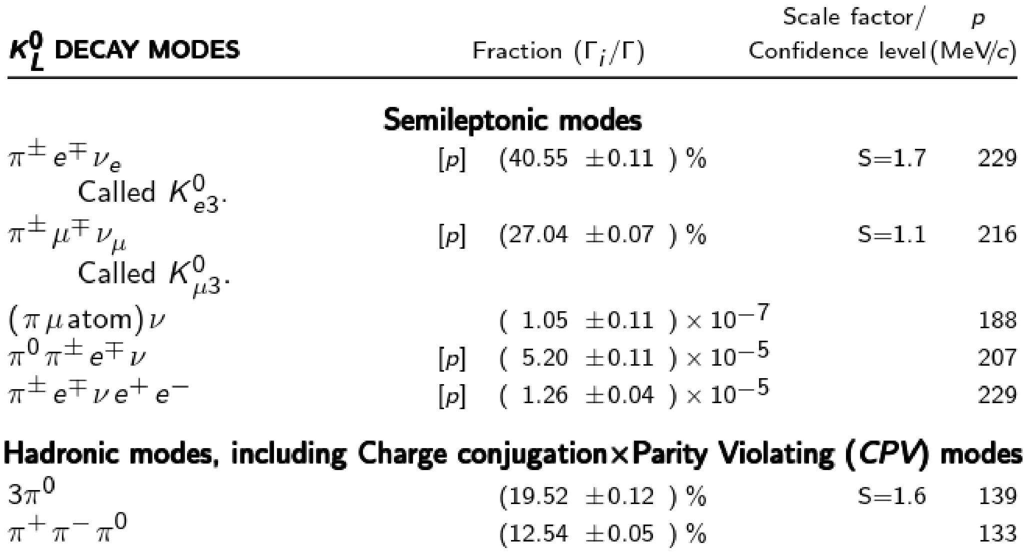

K_L^0 DECAY MODES		Fraction (Γ_i/Γ)	Scale factor/ Confidence level	p (MeV/c)
Semileptonic modes				
$\pi^\pm e^\mp \nu_e$ Called K_{e3}^0.	[p]	(40.55 ± 0.11) %	S=1.7	229
$\pi^\pm \mu^\mp \nu_\mu$ Called $K_{\mu 3}^0$.	[p]	(27.04 ± 0.07) %	S=1.1	216
$(\pi\mu \text{atom})\nu$		$(1.05 \pm 0.11) \times 10^{-7}$		188
$\pi^0\pi^\pm e^\mp \nu$	[p]	$(5.20 \pm 0.11) \times 10^{-5}$		207
$\pi^\pm e^\mp \nu e^+ e^-$	[p]	$(1.26 \pm 0.04) \times 10^{-5}$		229
Hadronic modes, including Charge conjugation×Parity Violating (*CPV*) modes				
$3\pi^0$		(19.52 ± 0.12) %	S=1.6	139
$\pi^+\pi^-\pi^0$		(12.54 ± 0.05) %		133

Figure 6: Decay modes of K_L^0 meson

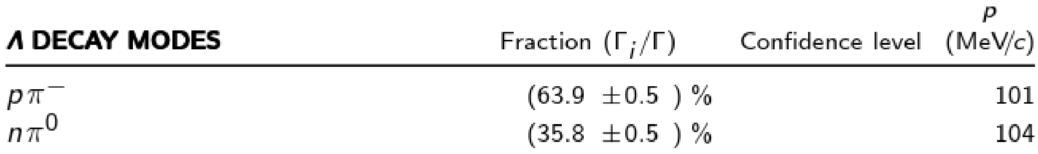

Λ DECAY MODES	Fraction (Γ_i/Γ)	Confidence level	p (MeV/c)
$p\pi^-$	(63.9 ± 0.5) %		101
$n\pi^0$	(35.8 ± 0.5) %		104

Figure 7: Decay modes of Λ^0 baryon

1.2 Regge theory and central diffraction

Regge theory is a framework developed in the 60s' by Tullio Regge [3]. It was originally used to describe strong interactions before QCD was formulated. It still remains relevant in places where perturbative QCD cannot be applied, for example in interactions with small momentum exchange. One of those cases are central diffraction (interpreted as Double Pomeron Exchange (DPE) process), which is governed by an exchange of so called Pomerons - particles described by aforementioned Reggie theory. In terms of lowest order QCD, a Pomeron can be described as a pair of gluons, with comparison to Regge theory shown on Figure 8 for the case of hadron pair production. The dark ovals visible on the graphics are example absorption effects, caused by interactions with other particles created during the process or with virtual particles. They are not important in this study, as the main properties of this reaction are still clearly visible.

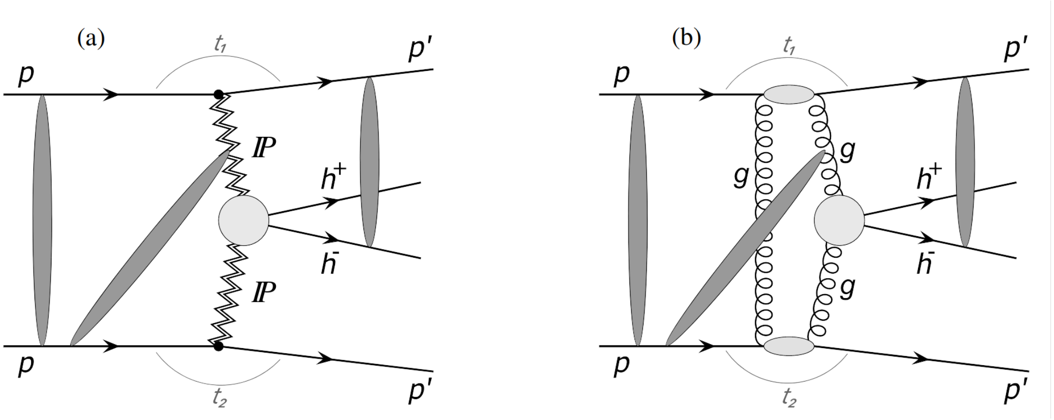

Figure 8: Exemplary model of non-resonant h^+h^- pair production by DPE in terms of (a) Regge theory and (b) leading order of petuberative QCD. Figures taken from [4]

Most notable properties of this Pomeron-driven central diffraction event are, among others, a survival of both protons and a rapidity gap between them and central state. This allows us to measure protons with Roman Pots (RP) detectors, and allows majority of created particles to be captured by central state detectors.

Above mentioned examples of DPE processes are the simplest one. In this thesis more complex final states are studied. The process under study is inclusive production K_S^0 and Λ^0 (or their decay products) where in addition to K_S^0 and Λ^0 decay products any other particles can be produced (detected or not) through the process called "fragmentation", which causes compound particles (like mesons or baryons) to be created from quarks and gluons created during collision. Additional particles produced might resemble K_S^0 and Λ^0 decay products, which makes it very difficult to separate them from actual decay products with kinematic cuts alone. Thus, we do not expect a clean signal in this analysis, and the peak in invariant mass distribution will always sit on top of continuous background. We can extract actual amounts of K_S^0 and Λ^0 produced by fitting the resulting distribution with gaussian peak with some sort of polynomial background added. Both K_S^0 and Λ^0 are made of strange quarks so their's presence in the final state is the signature of strange production in diffractive proton-proton collisions. The main motivation for this study is comparison of strange particle production expected from MC models like PYTHIA8 generator with measurements.

2 STAR Experiment at RHIC

The Relativistic Heavy Ion Collider (RHIC) is located at Brookhaven National Laboratory. It houses a few experiments (visible on Figure 9) and provides the ability to collide wide range of charged atomic nuclei (including several heavy elements, such as gold and uranium). Collision energies can achieve up to 200 GeV in case of nuclei, or up to 510 GeV in case of proton collisions. The protons could be polarised, which, while is not used in this thesis, is worth mentioning on it's own. RHIC will be decommissioned in the near future, and it's place will take Electron-Ion Collider (EIC), taking use of significant part of already existing structure.

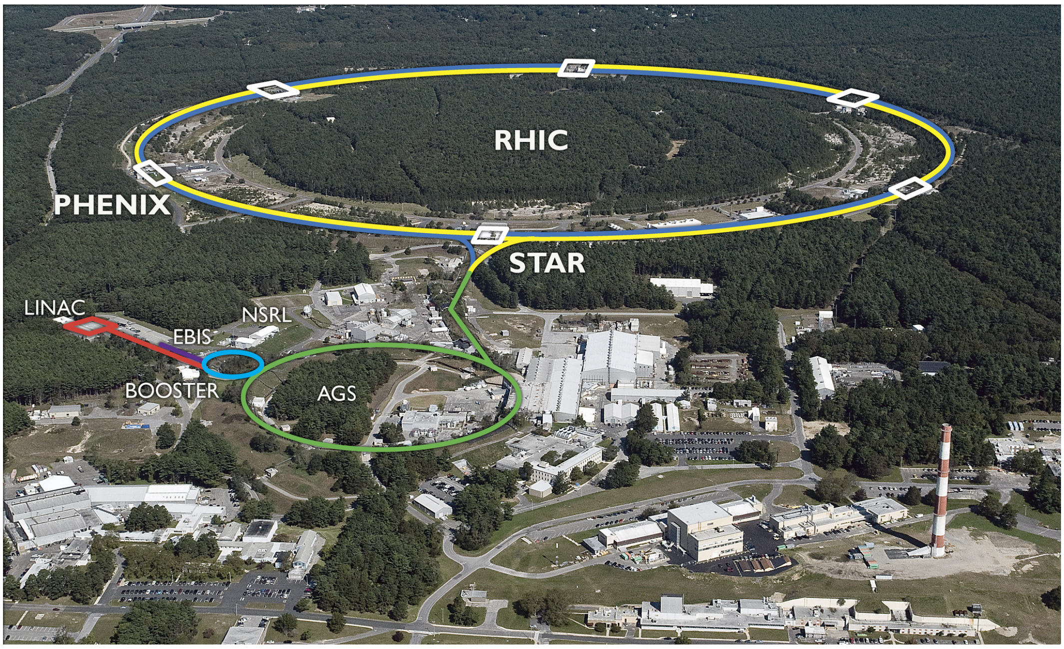

Figure 9: RHIC facility beamine layout, with most important facilities named.

The Solenoid Tracker At RHIC (STAR) experiment is a general-purpose detector fitted with multiple subsystems (Figure 10), including Time Projection Chamber (TPC), Time-of-Flight detector (ToF), Beam-Beam Counter (BBC) and slightly further from the interaction point, Roman Pots (RPs). Those will be the main instruments which were used for data acquisition for this thesis, which are not the only ones present in STAR, but the rest of them does not bear any significance to this analysis, thus their description will be brief. The central state detector is engulfed in 0.5 T magnetic field, parallel to the main axis, which allows to measure particle momentum by measuring the curvature of created tracks.

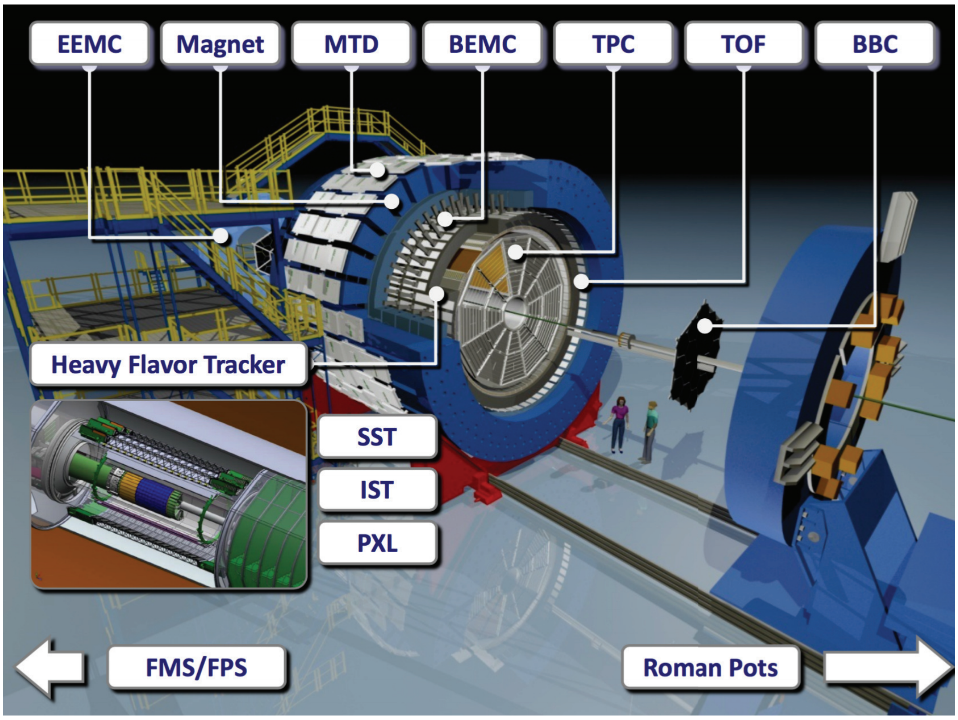

Figure 10: STAR detector layout. Figure courtesy of A. Schmah (STAR Collaboration).

The STAR detector consists of following components shown on Figure 10:

- EEMC (Endcap ElectroMagnetic Calorimeter) - used to measure the energy of particle that interact primarily via the electromagnetic interaction such as electrons, positrons and photons.
- Magnet - source of 0.5 T magnetic field, allows the measurement of charge particles momentum through their curvature in magnetic field, also used as shield to filter most particles except muons for MTD (below)
- MTD (Muon Telescope Detector) - Multi Resstive Plate Chamber, used mainly for triggering and muon detection
- BEMC (Barrel Electromagnetic Calorimeter) - scintillator-lead calorimeter, used for energy measurements of electrons, positrons and photons.
- BBC (Beam Beam Counter) - a set of scintillators placed near the beampipe, used for detection of charged particles.
- Heavy Flavour Tracker - used for detecting particles with heavy quarks and their decay products, consists of three similar components:
  - SST (Silicon Strip Detector)
  - IST (Intermediate Silicon Track)
  - PXL (PiXeL detector)
- FMS/FPS (Forward Meson Spectrometer) lead-glass Cherenkov for photon and electron measurement at high rapidity

- ZDC (Zero-Degree Calorimeter) - not present on picture, tungsten-based scintillating detector, used for detection of neutral particles scattered at very small angles.

2.1 Time Projection Chamber

The main part of STAR is Time Projection Chamber (Figure 11), a 4.2 m long cylindrical chamber of 0.5 m inside and 2 m outside diameter, with full azimuthal coverage and $|\eta| < 1.8$ longitudinal coverage. In practice, the region of high reconstruction efficiency is smaller, and spans a range of $|\eta| < 1$. It is filled with a 90%Ar-10%CH_4 gas mixture, which gets ionised as a result of a particle passing. The membrane in the middle, charged with high voltage (-28 kV), allows for the separation of electron-ion pairs, while endcaps, fitted with Multi Wire Proportional Chambers (MWPCs, Figure 12) allow positioning of the track in plane perpendicular to the beamline. Notable fact is that in this case, the electrons are used for measurement. Known drift speed allows to place the track in appropriate position along the beamline, allowing for full track shape reconstruction, which with coordination with magnetic field of the detector, allows momentum reconstruction. The energy loss while in the volume of detector allows for particle identification (PID) by comparing it with Bethe-Bloch formula for four species (e, p, π, K).

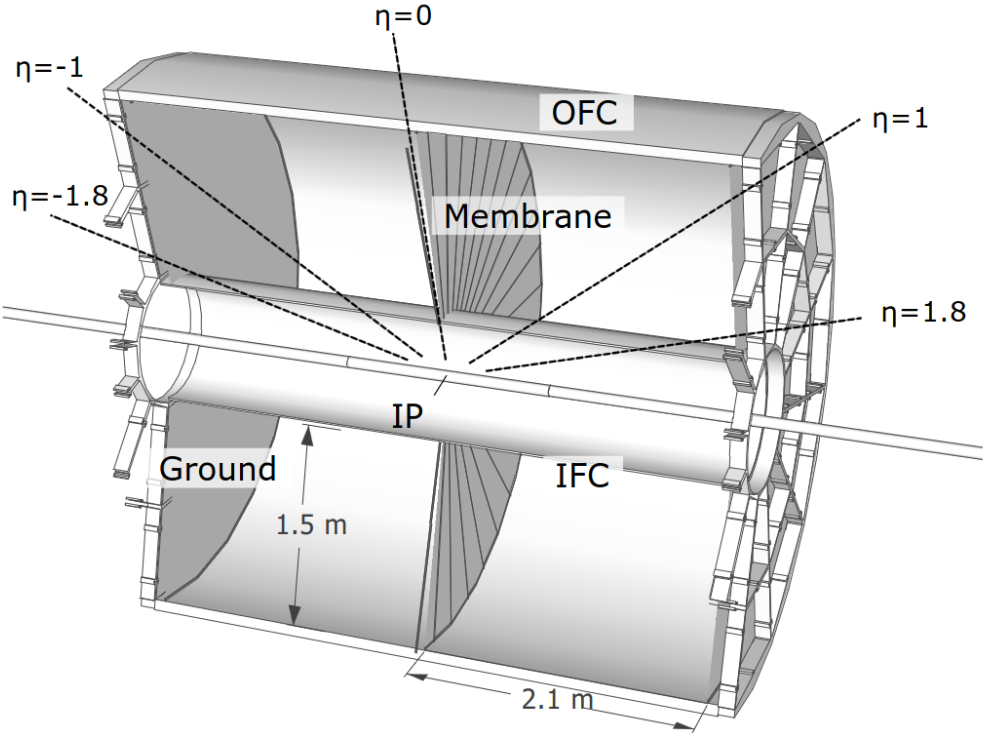

Figure 11: TPC barrel layout. Visible pseudorapidity for easier visualisation.

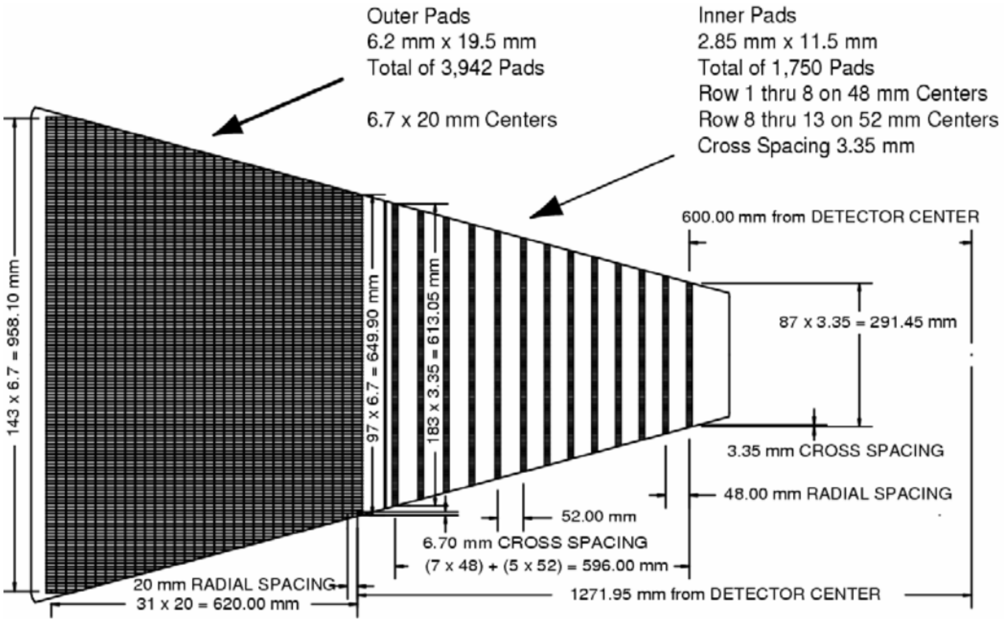

Figure 12: One of TPC endcap readout pads. Taken from [5]

2.2 Time-of-Flight detector

On the further edge of TPC detector, the Time-of-Flight detector (ToF) is placed. It consists of several modules of Multi-gap Resistive Plate Chambers (MRPCs, Figure 13), each set in it's own casing. Those trays were then arranged in a pattern along the TPC chamber, which was then radially copied. As you can see on Figure 14, they overlap each other, and those close to the ends are inclined - for better and more reliable coverage.

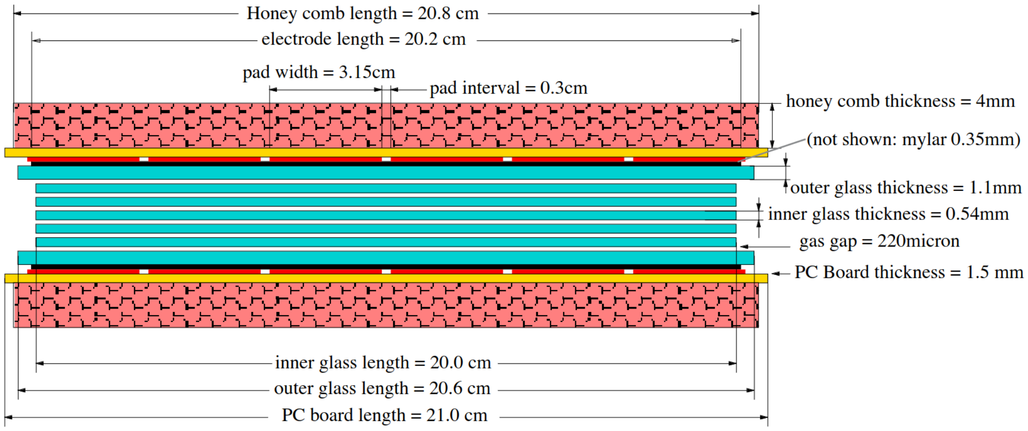

Figure 13: Time-of-Flight detector module: Multigap Resistive Plate Chamber. Figure taken from [6]

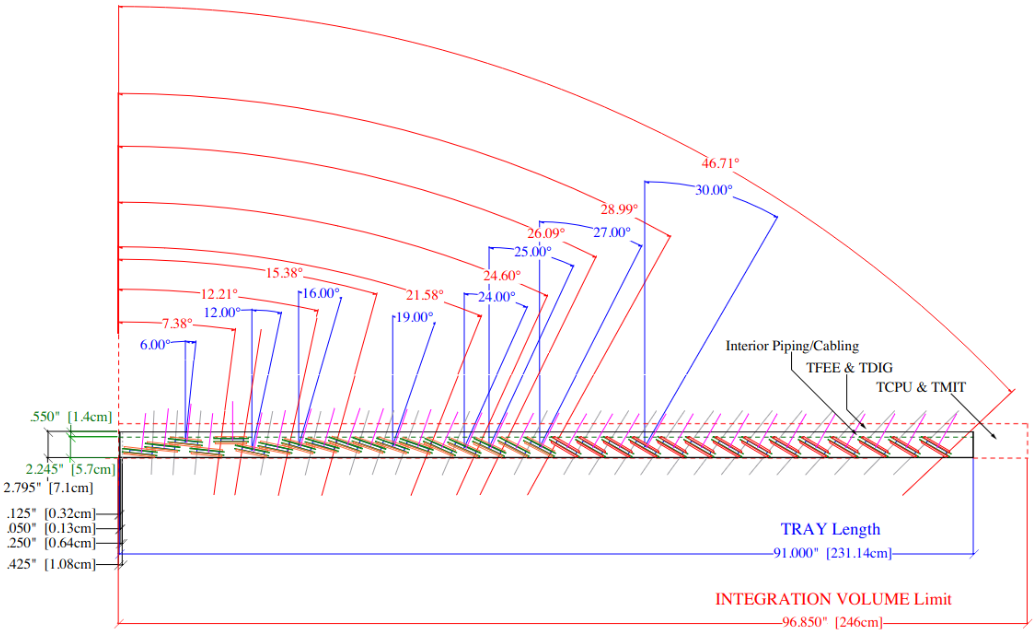

Figure 14: Tray of ToF modules. Modules are slanted to ensure best resolution. Figure taken from [6]

ToF covers the $|\eta| < 0.9$ region, providing timing information and additional PID capabilities. In this paper, it will be used for confirming existence of tracks reconstructed by TPC, as well as one of the trigger subsystems. An (unsuccessful) attempt will be made to use the timing information to identify decay products of K_S^0 particles.

2.3 Roman Pots

Roman Pot detector is a set of silicon-based strip detectors placed in 8 stations, along the beam path in groups of two in each station. Each detector consists of 4 planes, two with vertical and two with horizontal stripes, with strip width of 100 μm. Those allow us to collect data about transverse momenta of protons scattered at small angles around the beamline, with pseudorapidities in range of $7 < |\eta| < 9$. Due to their shape, they do not have full 2π azimuthal coverage. After the strip detectors, a plastic scintillator is placed, used as a trigger and for the timing information. The placement of Roman Pots is shown on Figure 15. DX and D0 are magnets used for beam control, while IP is the Interaction Point, where the collisions occur, and where we expect protons to come flying from. For ease of maintenance, they are placed in special kind of steel "vats", with 300 μm thick "window" for proton detection. Due to occasional service, they need careful alignment and sometimes additional calibration or data correction.

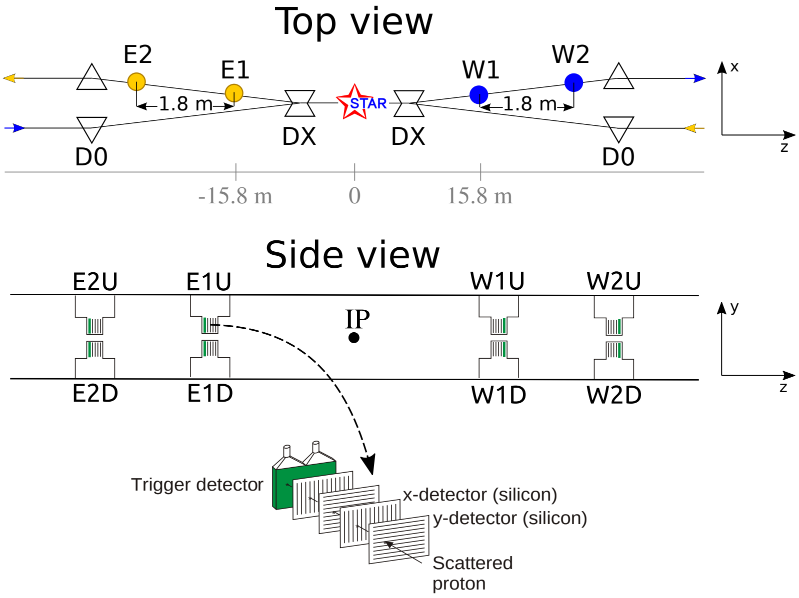

Figure 15: Roman Pots schematic placement and structure

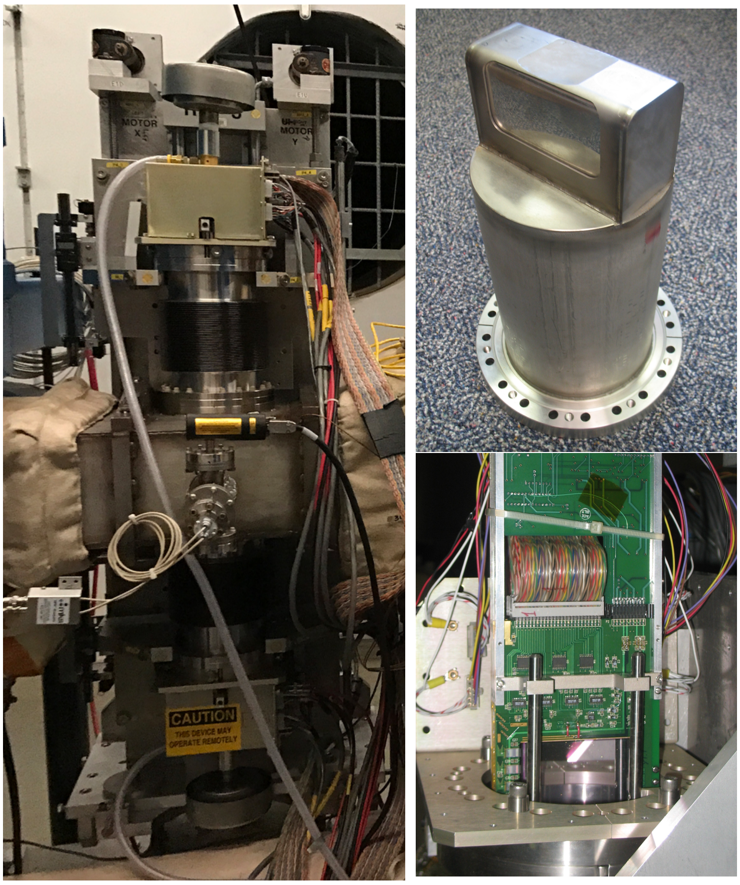

Figure 16: STAR Roman Pots. Left side - Roman Pot station. Upper right - protective shell, with 300 μm thick window visible. Lower right - detector electronics.

2.4 Beam-beam Counter

Beam-Beam Counter is a set of two kinds of plastic scintillators (Figure 17), placed at the end cap region, with larger ones covering the region of $2.1 < |\eta| < 3.3$ and smaller ones $3.3 < |\eta| < 5$. Although they are usually used in measurements of polarised protons, in this case they'll provide mainly trigger information and allow for data separation between large and very large rapidity gaps. Due to the rapidity gap existence in DPE-driven interactions, we do not expect to see any particles in the inner (BBC Small, or BBCS) ring of detectors and only few in the outer (BBC Large, or BBCL) . Due to different backgrounds and conditions of detection, events with and without signal in BBCL will be considered separately.

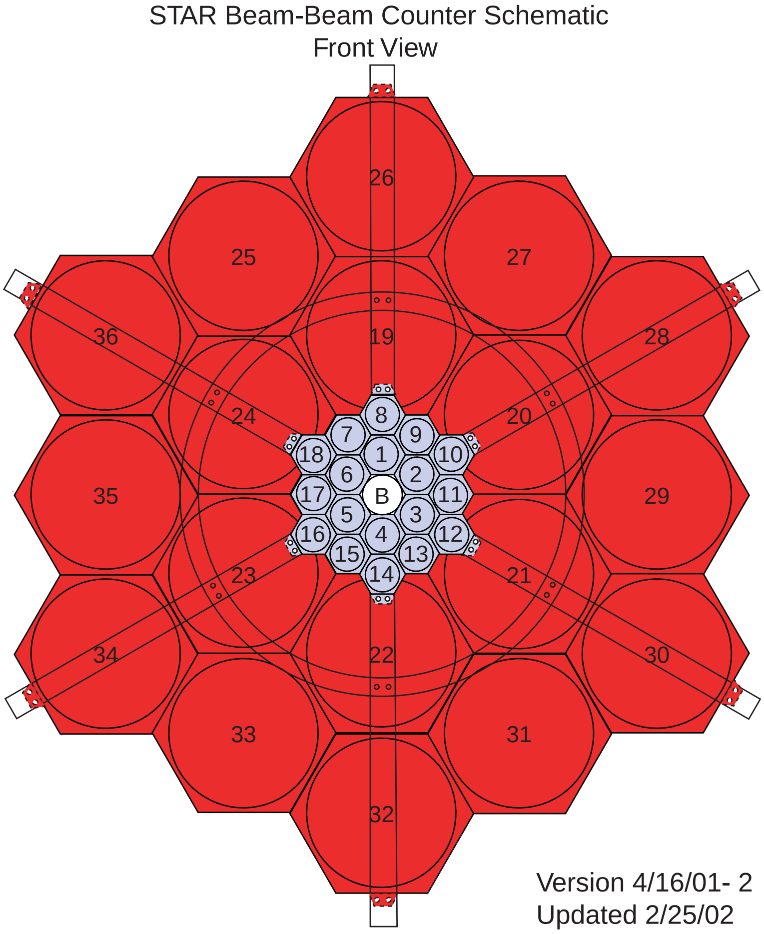

Figure 17: BBC detector. Visible inner 18 cells (blue) and outeer 18 cells (red).

3 Data analysis

The aim of this analysis was to measure cross sections for diffractive K_S^0 and Λ^0 production in $p + p \rightarrow p + p + K^0(\Lambda^0) + X$ process, as a function of various kinematic variables, such as transverse momentum and rapidity of $K^0(\Lambda^0)$ or relative momentum loss (ξ) of protons. Due to lack of detector effects corrections, so far the uncorrected diffractive yields were obtained.

3.1 Naming convention

Particle detection and tracks reconstruction is a vital process for this analysis. For clean description of the situation some explanation of track detection is needed.
First step is detecting particles flying through TPC active volume. Particles travelling through TPC leave along their path pockets of ionised gas, which then travel to endcaps where their XY position is measured by reading out pad charge, and their Z position by timing when they arrive. From TPC description [5] we see that pad size, drift velocity and a few other parameters were optimised so that the diffusion is roughly the same in both XY plane and Z direction ($\sigma_T = 3.3$ mm and $\sigma_Z = 5.2$ mm). The reading resolution, which, while dependant on charge deposited into pads and a few other aspects, remains roughly the same order of magnitude. Each of those reconstructed points will be called a "hit".
After collecting all hits, the process of event reconstruction begins, roughly described at Figure 18.

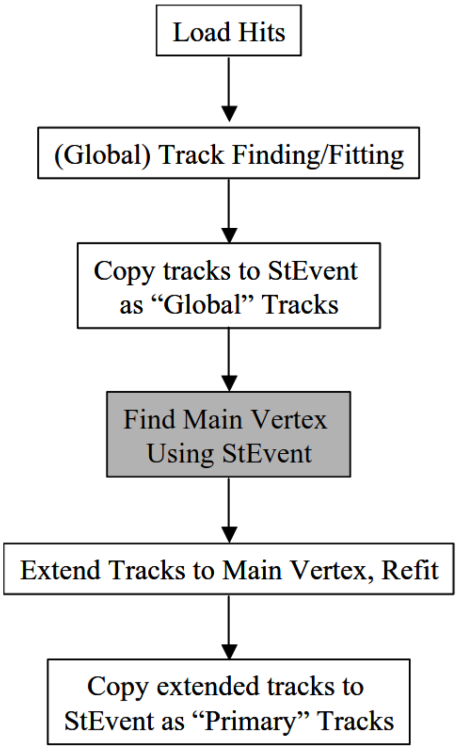

Figure 18: Schematic pipeline of reconstructed track processing. Taken from [8].

Fitting starts from the outer edges of TPC, where a few "track seeds" are found - short (a few hits) pieces of track to roughly estimate curvature, dip angle and other parameters. Track fitting is heavily reliant on Kalman filter[8], and after starting from the outside, adds hits to the track iteratively, minimising the χ^2 track statistic. Those tracks are saved as so called "global" tracks. After all tracks are identified, the Primary Vertexes (PV) are reconstructed. They are points where at least two global tracks are close enough to be considered as originating from the same point. In addition the position of PV must be close enough to the beamline to be considered as a candidate for collision vertex where two protons collide and central state is produced. We may have few PV in single events. It is due to the pileup of two or more collisions or presence of decay vertex which occurs close to beamline. After PVs are reconstructed, global tracks close to it are refitted including the PV position as one of the "hit. Those are then copied and rebranded as "primary" tracks, while all the other tracks are deemed "secondary".
This is where the problems begin, as both K_S^0 and Λ^0 have short decay lengths. In conjunction with imperfect momentum reconstruction (p_T resolution for magnetic field 0.25 T visible on Figure 19) this makes it very probable for tracks of decay products of aforementioned particles to be misinterpreted as primary tracks and therefore have even more improperly reconstructed momentum by including PV, which also has misreconstructed position due to including particles that did not originate from it. This of course leaves us without PV and possible cuts for it (as in, the central position of PV in detector or sufficiently small position difference between the one read by TPC and the one reconstructed from RP timing information). To avoid above problems K_S^0 and Λ^0 candidates are search for using global tracks or primary tracks without PV constrain in the fitting procedure. The search is performed by so called V0 finder, where V0 stands for neutral particle decaying into two charged particles (like K_S^0 and Λ^0)

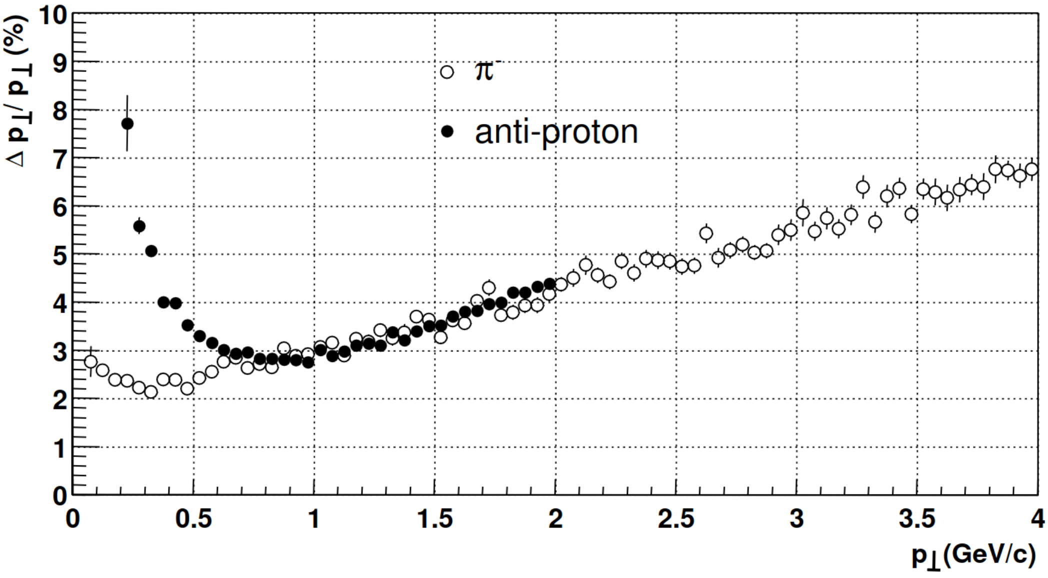

Figure 19: Transverse momentum resolution. Mag. field = 0.25 T, tracks had to have at least 15 hits. Taken from [5].

3.2 Kinematic variables and V0 finder

By applying cuts to variables describing a track of a particle, we can cut off badly reconstructed particles and narrow down a set from which K_S^0 and Λ^0 will be reconstructed. Variables used are not only kinematic ones, but also depend on detector characteristic of a track, such as number of hits used to reconstruct it. Those used in this analysis are as follows:

- p_T (transverse momentum) - a part of momentum perpendicular to the beamline
- $\eta = -\ln\left(\tan\left(\frac{\theta}{2}\right)\right)$ (pseudorapidity) - variable correlated with speed along the beamline
- N_{Hits} - number of hits used to fit the track.

Those variables are used in cuts for a singular track - to reconstruct decayed particle we need two of them. This both introduces us to new variables the cuts are possible on, and leaves us with the need of arranging it. The V^0 finder is a special class that uses data of tracks helices and combines two of them to allow us to reconstruct a decayed particle. During the process, new kinematic variables are introduced ,schematically drawn on Figure 20:

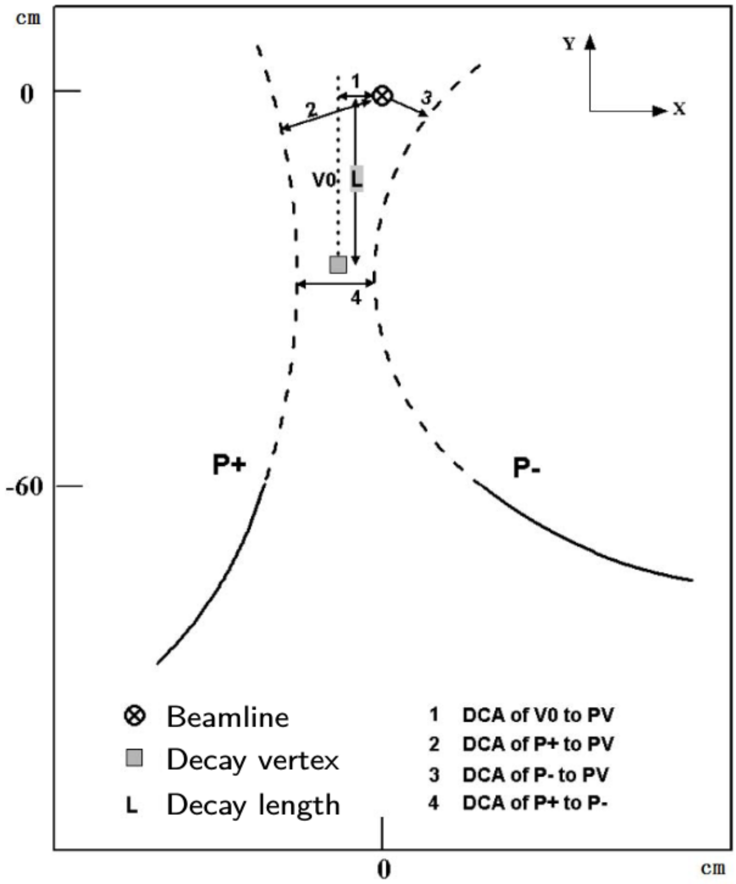

Figure 20: Schematic of tracks and new kinematic variables introduced by V0 finder. Taken from [9].

Four of those will be used for data filtering (DCA - Distance of Closest Approach):

- dcaDaughters (DCA of V^0 decay products)
- DCABeamLine (DCA of V^0 flight path to the beamline)
- pointingAngleCosine (Angle between flight path and momentum vector)
- decayLength (Distance between PV and decay vertex)

To work, V0 finder needs data about exact beam position, which are included in the events.

3.3 Data storage and processing

The STAR experiment stores detector data and physical information about detected particles in a microDST ROOT file format (DST stands for Data Storage Tag). Due to limited data storage and processing capabilities, additional data structure was created (picoDST) with reduced physics information for use in further analysis. For specific branches of analysis, even smaller structures are created, such as upcDST (used for Ultra-Peripheral Collisions). In comparison with picoDST, upcDST contain RP data not present in picoDST, but only a part of the TPC tracks correlated with primary vertices (vertices reconstructed at distance shorter than 3 cm from the beamline). This makes it very difficult to reconstruct all particles with relatively long decay lengths (such as K_S^0 or Λ^0). To increase efficiency of K_S^0 and Λ^0 reconstruction a special procedure were developed to extract all TPC tracks which may form K_S^0 or Λ^0 from picoDST and to merge them with standard upcDST samples (the so called extended upcDST). All additional tracks were decorated with flag (kV0), which stands for track being potentially decay product of $V^0 = K_S^0(\Lambda^0)$. Following selection criteria was used to extract track from picoDST and decorate it with kV0 flag:

- For each track:
    - $N_{Hits} \geq 15$
    - $p_T > 0.15$ GeV
    - $|\eta| < 1.1$
- For tracks pair forming V^0:
    - Total charge = 0
    - dcaDaughters < 2.0 cm
    - DCABeamLine < 2.0 cm
    - angle between line from collision vertex to V^0 decay vertex and direction of reconstructed V^0 momentum (ignored if V^0 decay happened in too short distance from collision vertex to properly estimate the angle): (pointingAngleCosine>0.9 or decayLength < 3.0 cm)
    - invariant mass (m_{pair}) of V^0 candidate being close to the nominal masses of V^0 particle, m_{K^0} or m_{Λ^0}: $|m_{pair} - m_{K^0}| < 0.035$ GeV or $|m_{pair} - m_{\Lambda^0}| < 0.015$ GeV

Cuts for elastic *pp* collisions were taken using the standard upcDST data, as they were available back then and nature of those cuts makes repeating analysis with extended upcDST redundant. This is the case also with some of the central state cuts - some of them were removed, as they were deemed ineffective.
After extending the upcDST data with additional tracks, the signal we got (comparison on Figures 21 and 22) is much higher than the one before.

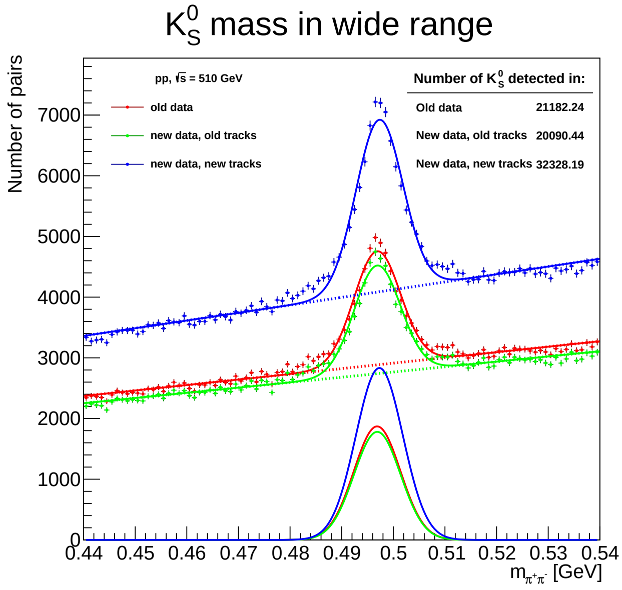

Figure 21: Comparison of K_S^0 detected between old and new data. Red and green plots should be overlapping, the difference is caused by the small change in preselection.

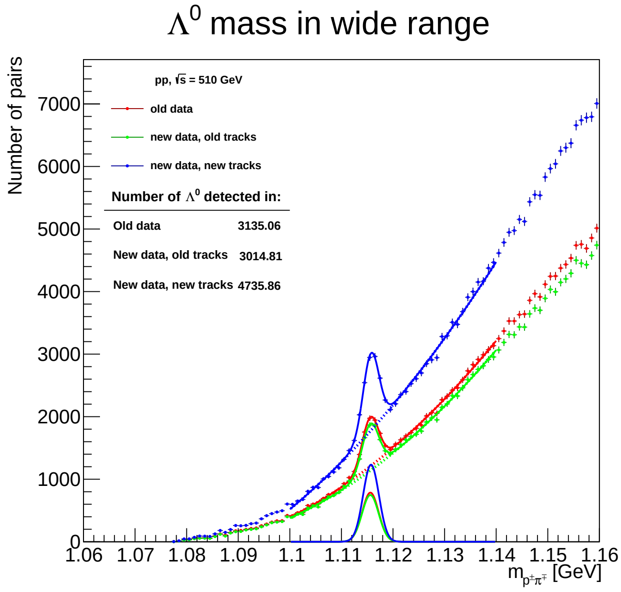

Figure 22: Comparison of Λ^0 detected between old and new data. Red and green plots should be overlapping, the difference is caused by the small change in preselection.

Given that Λ^0 has three times larger decay length, the products of its decay have very slim chance to be misidentified as primary tracks. Thus, we expect much bigger difference in K_S^0 yield than in Λ^0, and it is unclear why track change from local to global caused almost equal gain. The standard upcDST data (red) and primary tracks in new data (green) are the same hits and thus should be equal - a slight disparity occurred because of slightly different preselection rules (mainly demanding kV0 flag).

3.4 Fiducial region of the measurement

To ensure good proton track quality and large reconstruction efficiency the RP fiducial region was established. The shape of fiducial region was taken from exclusive central diffraction analysis done at collision energy $\sqrt{s}$ =200 GeV[4] and then scaled from $\sqrt{s}$ =200 to $\sqrt{s}$ =510 GeV (see Figure 23). Final values used for cuts in the analysis are as follows:

$$\begin{cases} p_x > -0.27 \text{ GeV} \\ 0.8 \text{ GeV} > |p_y| > 0.4 \text{ GeV} \\ (p_x + 0.6 \text{ GeV})^2 + p_y^2 > 1.25 \text{ GeV}^2 \end{cases}$$

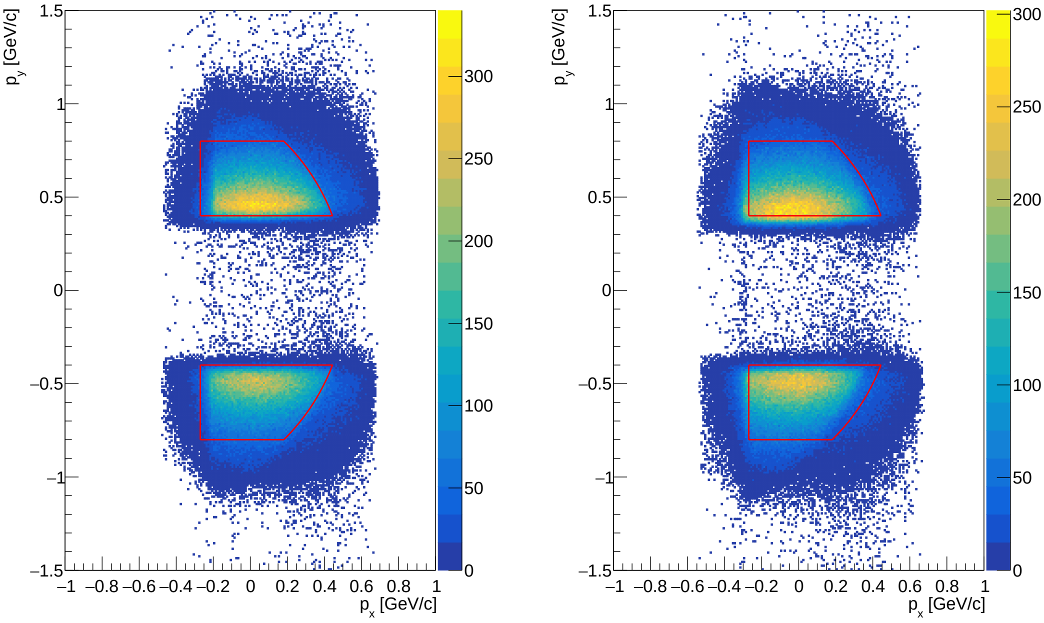

(a) West RPs

(b) East RPs

Figure 23: Momentum of protons reconstructed in Roman Pots. Fiducial cut marked with a red line.

Furthermore, simulations using PYTHIA8 [7] generator were made, and they allowed to restrict fiducial region even more, cutting off regions in ξ with low acceptance to detect charged particles in TPC and pass BBCL veto.

PYTHIA8 has an option to simulate central diffraction events exclusively, which allowed for better sample sizes (effects of the simulation visible on Figure 24 were achieved by simulating 10 million events). Furthermore, while there was no option to choose production of events containing at least one K_S^0 or Λ^0, there was one to choose the channel of decay, which brought down the needed amount of simulated events even more.
The events simulated (after confirming they do contain K_S^0 or Λ^0 which we might actually detect) were put through a series of cuts, simulating both the detectors and the cuts we used during the analysis. The geometrical acceptance of the detectors was simulated by setting following conditions:

- TPC & ToF detectors
  - $p_T > 0.2$ GeV
  - $|\eta| < 0.9$
  - particle had to be charged
  - particle had to be "Final" - it won't decay further in the simulation
- BBCL
  - $p_T > 0.5$ GeV
  - $2.1 < |\eta| < 3.3$
  - particle had to be charged
  - particle had to be "Final"

As the simulation was done to estimate ξ-dependant fiducial region of high acceptance of TPC and BBCL veto, for higher statistics reconstruction efficiency was assumed to be 100%. The RP geometrical acceptance was implemented by applying RP fiducial cuts. Full list of cuts applied in this simulation is as follows:

- RP fiducial cuts
- RP anti-elastic cuts for ξ and p_{XY}
- No particles in BBCL
- At least 2 particles in TPC & ToF
- At least one opposite-signed pair

The result of this simulation is visible on Figure 24. The colour scale represents ratio of central diffractive events containing K_S^0 or Λ^0 after and before applying requirements for TPC and BBCL veto

This allowed us to define two possible fiducial regions:

- Red, based on rectangle shape in ξ:
  - $0.005 < \xi_E < 0.08$
  - $0.005 < \xi_W < 0.08$
- Green, based on rectangle like shape in mass and rapidity of the central state[1]:
  - $2\log(0.005) < \log(\xi_E \cdot \xi_W) < 2\log(0.08)$
  - $|\ln(\xi_E/\xi_W)| < \ln(0.005/0.08) = 2.77$

After accidental background analysis, decision was made to use the red cuts since they better fit with anti-elastic removal cuts. For data sample taken without BBCL veto, slightly larger fiducial region is taken ($0.005 < \xi_{E,W} < 0.2$ because BBCL veto affects only high ξ events (large diffractive masses). This is visible on Figures 25 and 26 where ξ distributions observed in data are presented, respectively for events taken without and with BBCL veto.

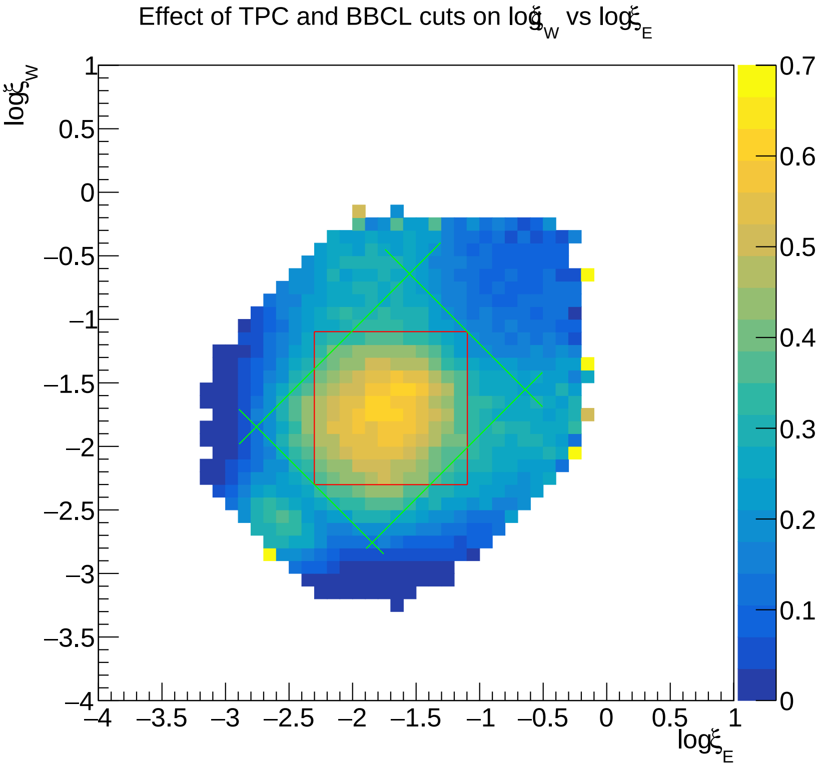

Figure 24: Efficiency of detection of central diffractive events after taking into account finite dimensions of TPC and BBCL detectors. Two suggestions of ξ cuts overlayed.

---

[1] $\frac{M_X^2}{s} = \xi_E \xi_W$ and $y_X = \ln\left(\frac{\xi_E}{\xi_W}\right)$, where M_X is the mass of central state, and y_X its rapidity

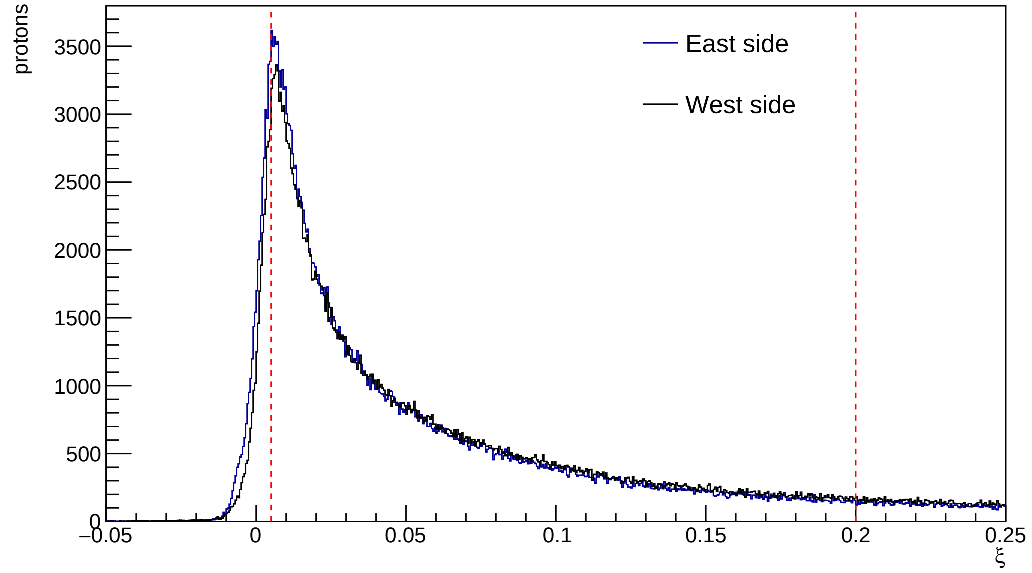

Figure 25: Histogram of ξ taken from events from RP_CPT2 trigger with K_S^0/Λ^0 detected. Cut lines are shown.

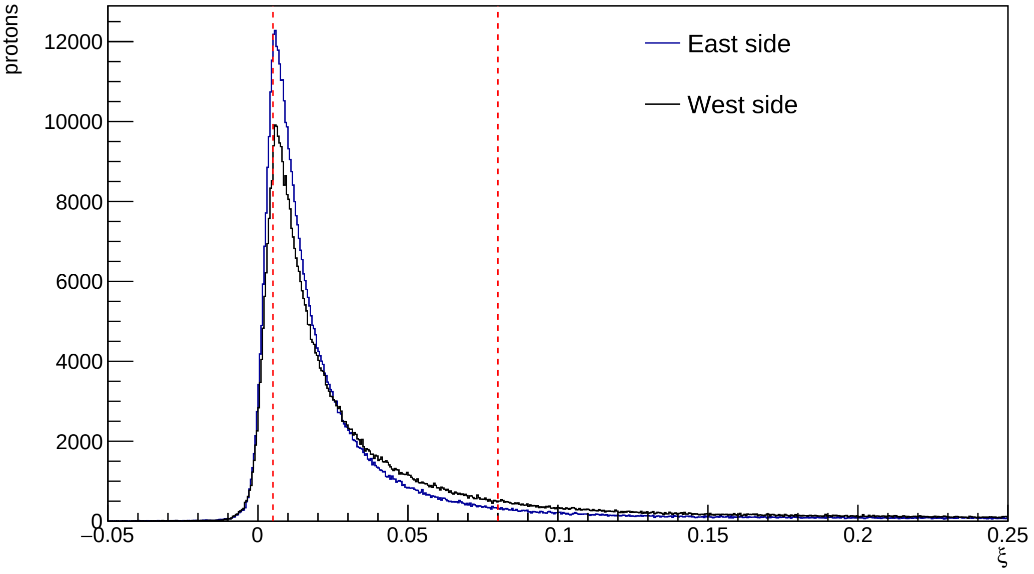

Figure 26: Histogram of ξ taken from events from RP_CPT2noBBCL trigger with K_S^0/Λ^0 detected. Cut lines are shown.

3.5 Accidental background

Main source of background for central diffractive events is an accidental overlap of elastic scattering process with activity in central detectors caused mainly by non-diffractive processes. This background is visible as a peak at low ξ values shown on Figure 27. The origin of the peaks is confirmed by ξ distribution obtained from zero-bias trigger applying the same cuts on forward protons as used in the selection of central diffractive events.

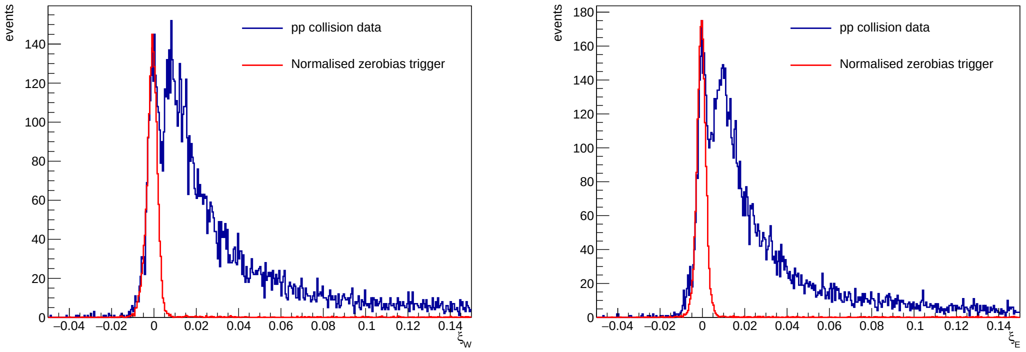

(a) West RPs

(b) East RPs

Figure 27: Proton ξ distributions, for west (left) and east (right) sides. Results recorded by zero-bias trigger were normalised to central production data and overlayed.

3.5.1 Elastic collision removal

Elastic protons are expected to peak at zero in ξ, sum of transverse components of protons momenta ($\sum p_x$ and $\sum p_y$) and sum scattering angles ($\sum \theta_{XZ}$ and $\sum \theta_{YZ}$). To compare with central production data, a zero-bias trigger was used to obtain pure elastic collision events sample. Those were then analysed in three ways (ξ_E vs. ξ_W, $\sum p_x$ vs. $\sum p_y$, and $\sum \theta_{XZ}$ vs. $\sum \theta_{YZ}$), and a gaussian peak was fitted in all three cases. Considering cut on $\sum \theta_{XZ}$ vs $\sum \theta_{YZ}$ as similar in effect to the $\sum p_x$ vs. $\sum p_y$ one, for data analysis only $\sum p_x$ vs. $\sum p_y$ and ξ_E vs. ξ_W cuts were used, and 3σ region around peak was chosen. Comparison of all of them is shown on Figure (28).

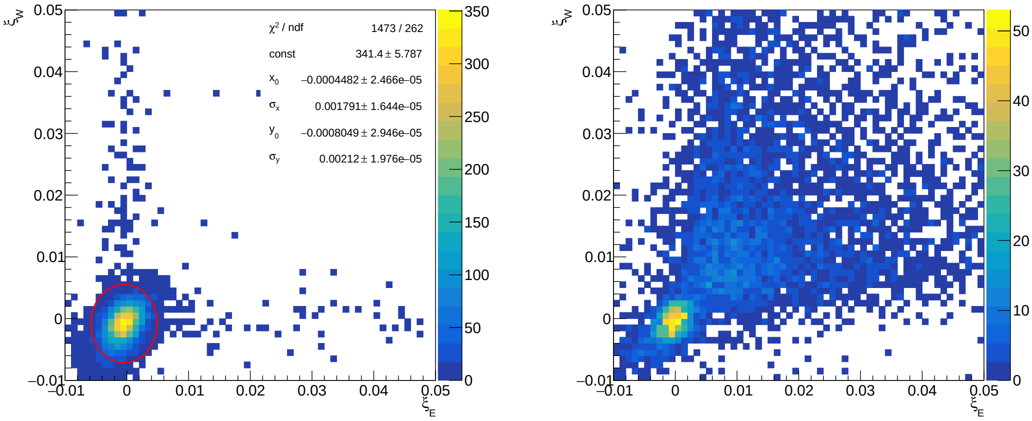

(a) ξ_E vs. ξ_W, zero-bias trigger

(b) ξ_E vs. ξ_W, CPT2 trigger

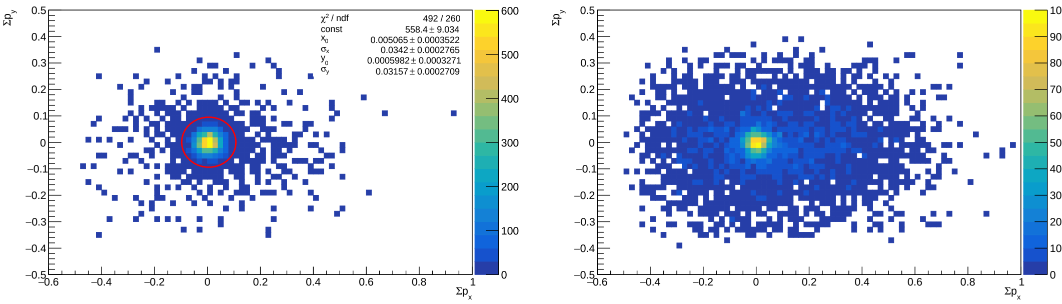

(c) $\sum p_x$ vs. $\sum p_y$, zero-bias trigger

(d) $\sum p_x$ vs. $\sum p_y$, CPT2 trigger

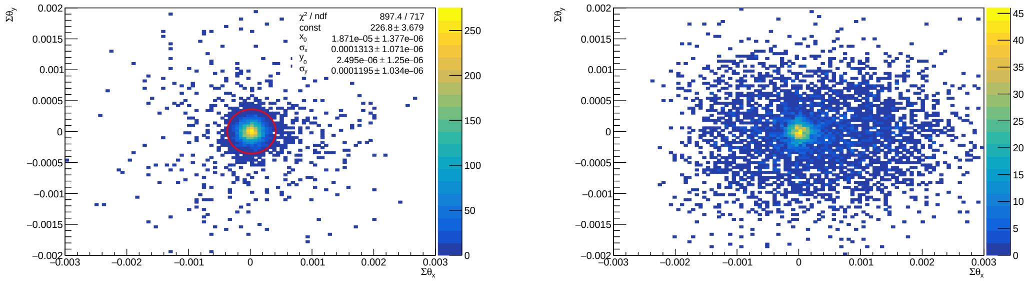

(e) $\sum \theta_{XZ}$ vs. $\sum \theta_{YZ}$, zero-bias trigger

(f) $\sum \theta_{XZ}$ vs. $\sum \theta_{YZ}$, zero-bias trigger

Figure 28: Left - Distributions for protons from zero-bias trigger, with cut from fitting gaussian peak overlayed on them, right - distributions from CPT2 triggers, on which the cut will be used. Clearly visible elastic peaks in all three of them.

3.6 Initial preselection

Due to large volume of data recorded, a preselection of events was needed, which was conducted on the STAR servers. All histograms were created after the preselection, in an "n-1" fashion - all cuts are applied except the tested one, to see how that particular cut affected the data. Following subsections describe the preselection procedure.

3.6.1 Preselection of triggers

Triggers are a set of simple and fast to detect conditions (such as number of particles in given detector or particularly high energy measured) that allow us to decide whether an event is important for further analysis at the time when experiment is running. Events which do not pass trigger conditions are lost and not available for physics analysis. For this analysis three triggers were used:

- RP_CPT2 (trigger number 570701), up to run 18083025
- RP_CPT2noBBCL (trigger number 570705), after run 18083025
- RP_zerobias (trigger number 570704)

They filtered the data according to following rules:

- RP_CPT2:
  - Signal only in one of two RP branches on either side
  - No signal in BBC (small tiles) or ZDC on either side
  - At least 1 and no more than 10 hits in TOF
- RP_CPT2noBBCL:
  - All of RP_CPT2 requirements
  - No signal in BBC (large tiles)
- RP_zerobias:
  - Random (zero-bias) trigger

In the preselection first two of those were used for collection of central diffractive events, while the last one was used to study accidental overlap of elastic process ($p + p \to p + p$) with any activity in central detectors which form a background for central diffractive events.

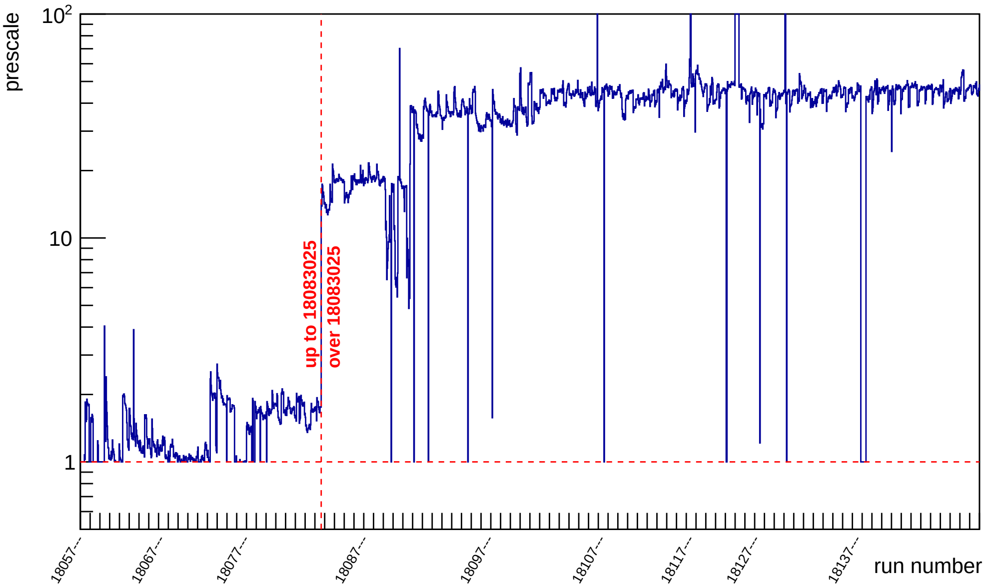

Figure 29: RP_CPT2 trigger prescale as a function of the run number. Visible line for scaling 1 and for run with sudden change.

In general each trigger can be scaled (only a fraction of triggered events is stored) to keep event rate at acceptable level. Trigger prescaling of n means 1 of every n events matching the criteria is recorded. Ideally trigger prescale should be 1. At early stage of data taking in 2017 year the effective prescale for trigger RP_CPT2 was around two as seen on Figure 29. Therefore from run 18083025 new (more restrictive) trigger, RP_CPT2noBBCL, was introduced while RP_CPT2 was prescaled by 15-50 and kept for monitoring. This change was optimal for main physics goal (exclusive production) however introduced some limitation of the kinematic phase space available for inclusive processes studied in this analysis.

3.6.2 Preselection of central diffractive events in RP detectors

In central diffraction processes we expect to reconstruct single proton on each side of STAR detector. However due to the event pileup two or more protons can hit the detector. Furthermore RP is a set of strip detectors providing only one dimensional information. Two dimensional information is obtained by combining two perpendicularly oriented strip planes. This leads to the presence of fake protons as depicted on Figure 30(a) for the case of two real protons hitting the same station. To reconstruct proton track, information from two stations (2D points) are combined as shown on Figure 30(b). If in the first RP station n_1 2D-points are reconstructed, and in the second one n_2, then total number of protons candidates on that side is $n_1 \cdot n_2$ - each hit was connected to each other and proton candidate is reconstructed. Taking into consideration all those problems, the cut for one proton on each side was applied. The effect of rejecting multiple events does not affected any result presented in this thesis.

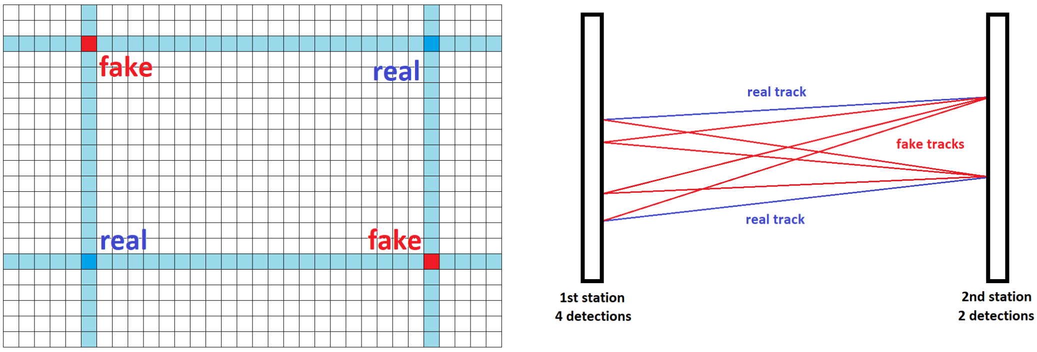

(a) Multiple detections

(b) Multiple tracks

Figure 30: Example of (a) multiple detected "ghost" protons and (b) multiple reconstructed tracks from RP data

Minimal number of planes to reconstruct proton position is two - one with vertical and one with horizontal orientation of strips. To eliminate possible errors where proton was only detected in two planes with the same direction of stripes, at least three are expected. Of course, four would be better, but given high efficiency of RPs and small difference between 3- and 4-plane hits, the cut for at least three hits in both stations in one branch is sufficient. In principle proton scattering angle can be reconstructed using only one RP station and position of Interaction Point. This is enough for measurements of elastic process or exclusive central diffraction were proton energy is equal or almost equal to the beam energy. However to reconstruct proton momentum two RP stations are required. For inclusive central diffraction such information is essential therefore only protons reconstructed from both stations are preselected.

3.7 Preselection of tracks reconstructed in central detectors

At this point of preselection, we can finally take care of tracks registered by central state detectors. Following conditions were required:

- For each TPC track:
    - Matching hit in TOF
    - Number of hits used for track reconstruction ($N_{Hits} \geq 15$)
    - Transverse momentum ($p_T > 0.15$ GeV)
    - Pseudo-rapidity ($|\eta| < 1.1$)
    - Having kV0 flag
- For each event:
    - At least two tracks passing above mentioned selection
    - At least one pair of opposite-charged selected tracks

3.7.1 Kinematic cuts

Due to limited detection capabilities and worsening the quality of reconstructed tracks at the edges, cinematic cuts for p_T and η were applied. TPC can properly reconstruct tracks with 0.1 GeV< p_T < 30 GeV and $|\eta|$ <1.8, however to keep the quality of reconstruction high enough, we reject tracks with p_T < 0.2 GeV or $|\eta|$ >0.9 - cuts visible on Figures 31 and 32.

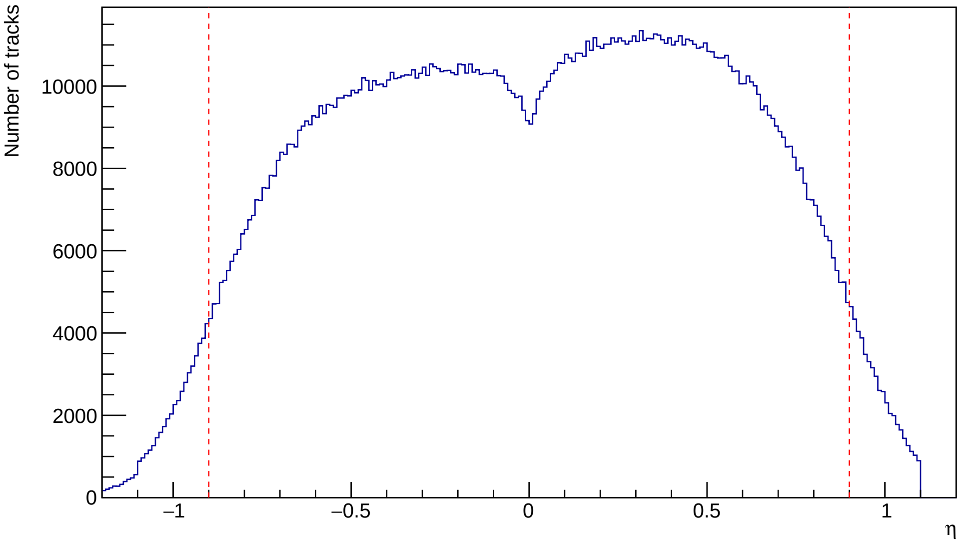

Figure 31: η track distribution. Cuts taken ($|\eta|$ >0.9) are marked by the red lines.

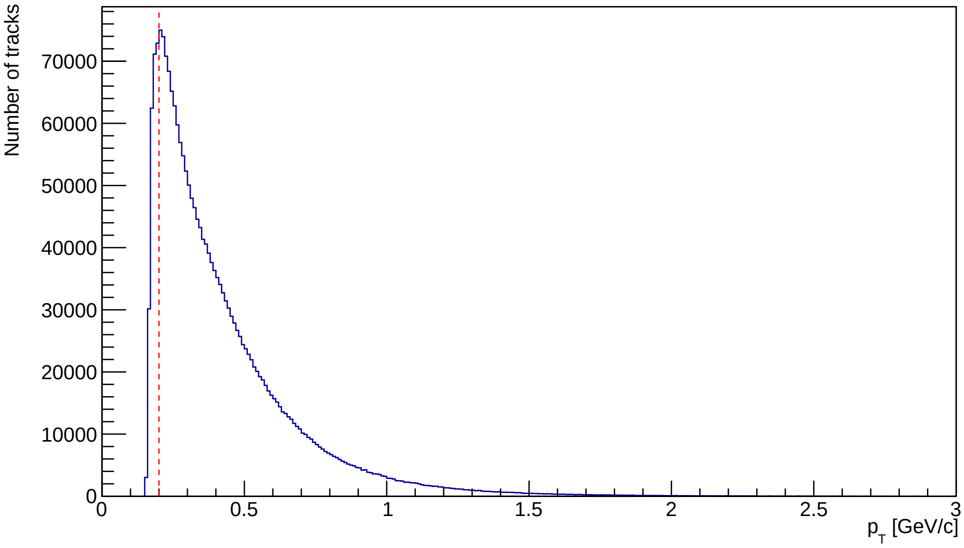

Figure 32: p_T track distribution. Cut for p_T > 0.2 GeV is marked by a red line.

On Figure 31 we can see a few very characteristic features:

- "Hole" at $\eta \approx 0$, due to existence of charged membrane messing with the tracks and their reconstruction
- Small drops at $|\eta| = 1.1$, caused by preselection and kV0 flag (asymmetry might be caused by improperly applied cuts, but, as the cut is more strict, it doe not matter)

Asymmetry in η distribution is thought to exist due to some sort of detector irregularity, and as such, it might cause imbalance in amount of reconstructed particles. On Figure 32 we can notice that although TPC can detect particles up from $p_T >$0.1 GeV, we get signal only from 0.15 GeV and up - this was caused by the preselection and kV0 flag enforcement.

3.7.2 TOF flag

ToF detector, apart from giving us (not useful for this analysis) timing information, allows us to confirm the existence of in-time TPC tracks. This helps us to clean the events from off-time pile tracks and other fake tracks. Every track that has a hit in ToF that matches with track in TPC gets a "kTOF" flag. Its existence allows us to separate them, as you can see on Figure 33. Unfortunately, according to [10] ToF efficiency is around 70%, which means not all tracks are recorded. Furthermore, there exists a possibility of only partial reconstruction of some tracks, which causes the number of tracks to spike up without actual separate, distinct particles existing.

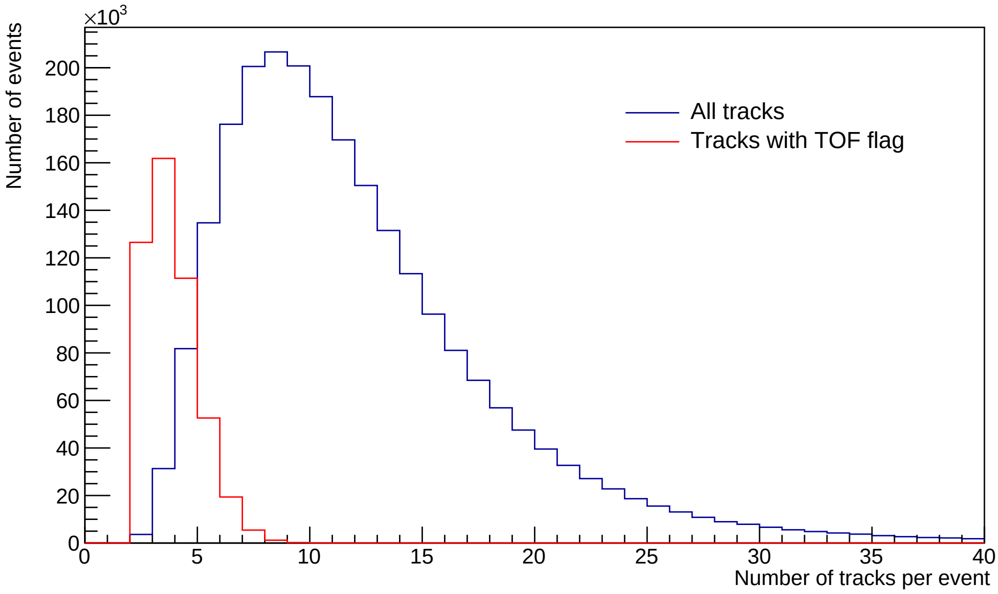

Figure 33: Multiplicity of tracks in an event.

3.7.3 Number of hits used for track reconstruction

TPC track finder starts from the outer edge, collecting a few hits close to each other, seeking the next one using straight line approximation until a set limit is achieved. This means that the algorithm can pick up pile-up tracks, some sort of tertiary tracks or tracks from electrons randomly generated during particle flight, which are generally not needed and only obscure the image we are trying to recover.

Thus, to further clear the data, a cut on number of points used to identify the track was taken (visible on Figure 34) - tracks with $N_{hits} > 20$ were used. The sharp cut on $N_{hits} = 15$ is here because of the preselection setting used. As particle identification was not used in this analysis, the cut for number of points used to estimate the kind of particle by energy loss was not used.

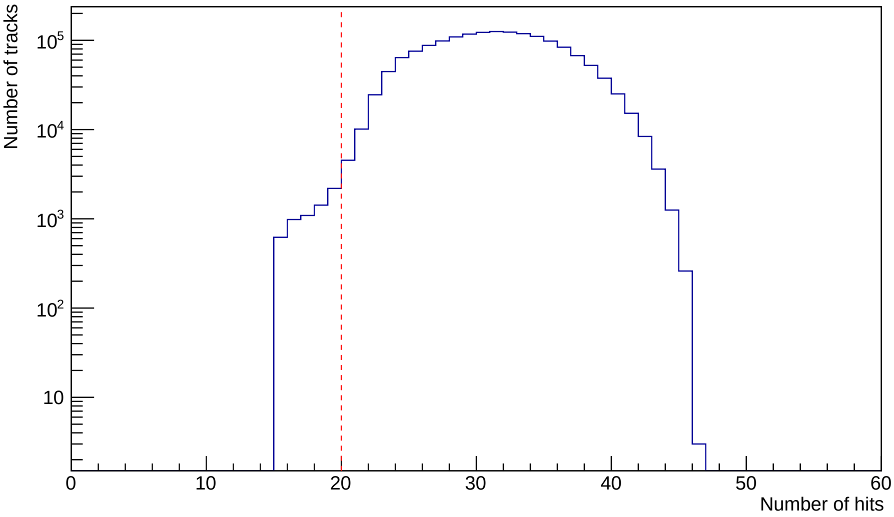

Figure 34: Number of clusters used for track reconstruction. Small number of hits means huge probability of track being badly reconstructed.

3.7.4 DCA to beamline

Because the PV was not reconstructed, we assume one exists, somewhere on the beamline. Beamline is parameterised using data taken from STAR database. Original particle momentum can be reconstructed as a sum of momenta of particles decaying from it, and given that both K_S^0 and Λ^0 are neutral, their momentum vector is parallel to their track (unaffected by the magnetic field TPC is in). Using this information, and the DCA of charged decay products (which is assumed to be the decay vertex of the particle), we were able to find the distance between the beamline and presumed path of the particle. Of course, a huge distance means that a pair that we assumed to be from one particle, is actually not, and as such, does not need to be taken into consideration. As such, a cut for DCA<2.5 cm was considered from MC simulations and applied, visible on Figure 35. The cut value is a reflection of detector resolution rather than physical process behind it.

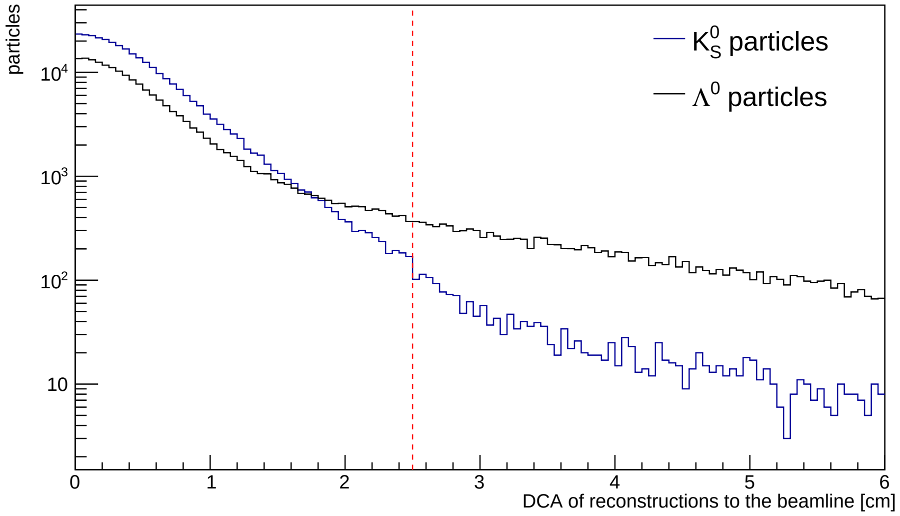

Figure 35: DCA of reconstructed particles. Cut applied is denoted by a red line.

3.7.5 DCA of decay products

The path reconstruction is not ideal due to the non-zero resolution of TPC detector. Ideally, the paths of decay products would intersect at the point of particle decay, and thus the two helices used to model their paths would intersect. However, in practice due to the aforementioned problems there exists a bit of a leeway. Thus, a cut for decay results' tracks can be made so that they lie sufficiently close to each other. By MC simulations, cut of DCA< 2.5 cm was deemed appropriate and used, as seen on Figure 36.

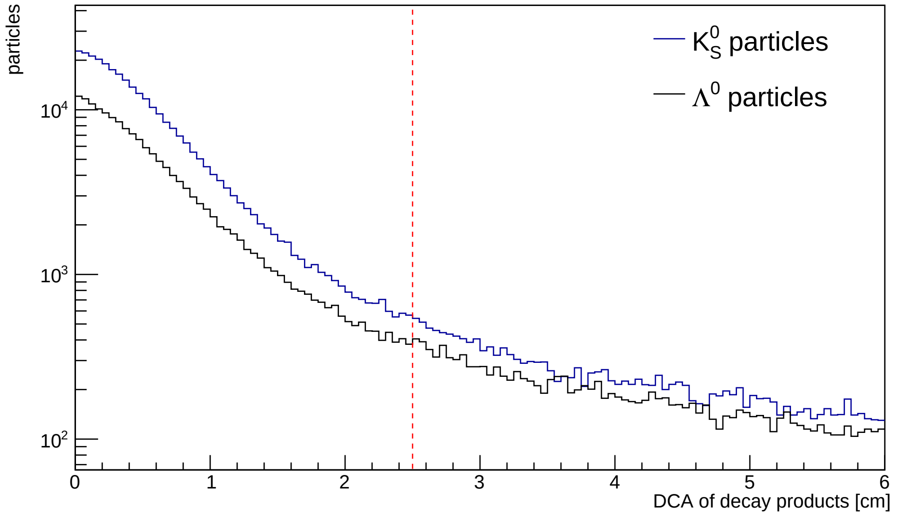

Figure 36: DCA of decay products. Cut applied is denoted by a red line.

3.7.6 Angle between flight path and PV-Decay vertex vector

Due to K^0 and Λ^0 particles being neutral ones, the magnetic field inside TPC does not affect them. This causes them to move in a straight line (due to their speed and lifetime gravity is negligible) from the point of production to the point of decay. The momentum should be parallel to this line, or at least (due to detector resolution) very close to it. Thus, a cut for an angle was made for tracks with longer decay length. Those with smaller one, due to difficulties of accurate reconstruction, were not subjected to it. The exact conditions are:

$$\text{pointingAngleCosine} > 0.925 \vee \text{decayLength} < 3.0\text{cm}$$

Cuts applied are visible on Figures 37 and 38. These cuts do not cut out much, because they are only a bit less lenient than those applied by demanding kV0 flag, but they cut out some of the background nevertheless.

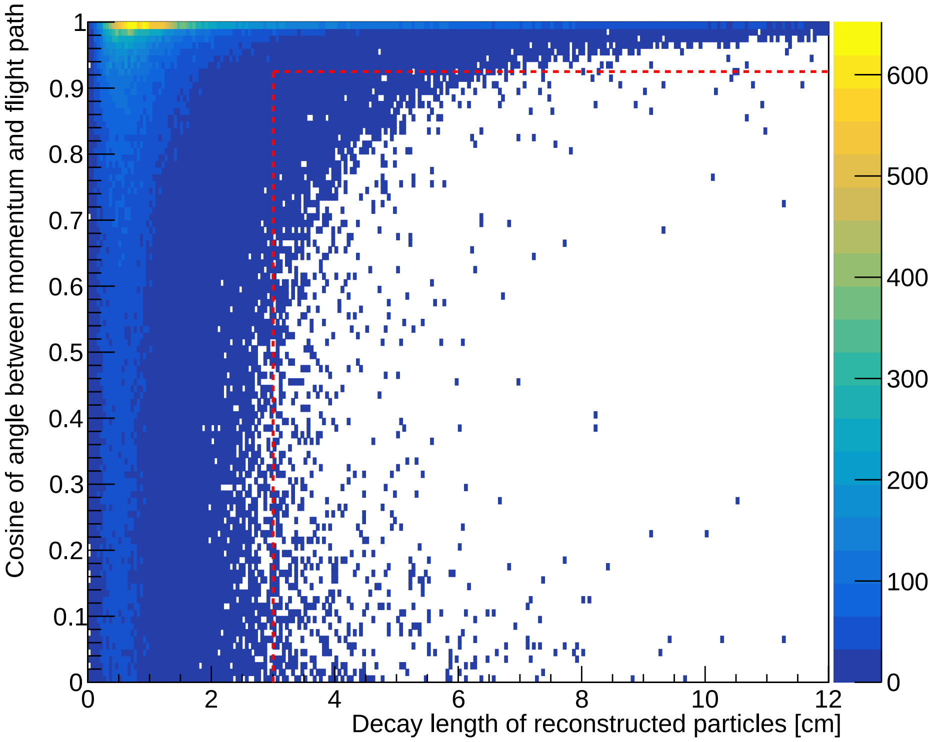

Figure 37: Histogram of compound cut on K^0_S. Lower right region is cut off.

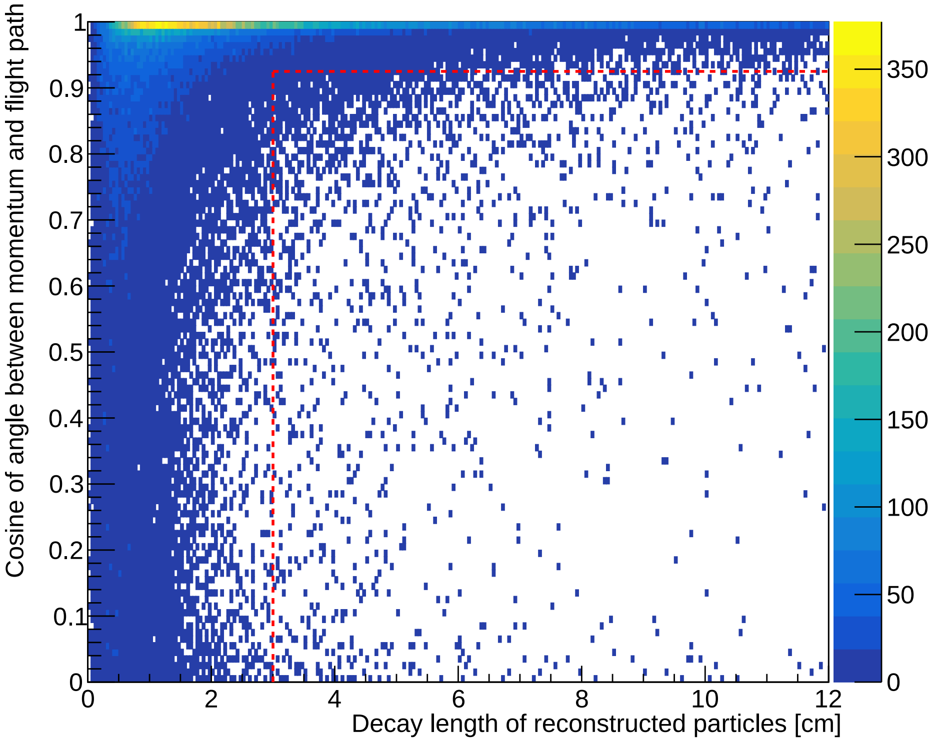

Figure 38: Histogram of compound cut on Λ^0. Lower right region is cut off.

3.8 Removal of duplicated tracks

After identifying all good quality tracks and pairing them, to make analysis quicker only resulting particles within "mass windows" defined around K_S^0 and Λ^0 masses are taken into consideration. Mass windows are defined as follows:

- 0.44 GeV< $m_{\pi\pi}$ <0.54 GeV for $\pi\pi$ pairs
- 1.06 GeV< $m_{p\pi}$ <1.16 GeV for $p\pi$ pairs

As the idea of particle identification was currently abandoned due to not getting good signal-to-background ratio, the masses of particles in pairs (needed to properly reconstruct decayed particle) were assumed as pion or proton mass. Due to the nature of this process, one positive-negative pair could be interpreted as three possibilities: $\pi^+\pi^-$ for K_S^0 reconstruction, or $p^+\pi^-/p^-\pi^+$ for Λ^0 reconstruction. Those pairs were then checked if they fit in the respective mass windows.

Of course, this process didn't protect from using one track to fit in multiple pairs. That was achieved by listing all created pairs by DCA between particles in ascending order, and pruning any pairs which used track previously used in pairing with smaller value. This step is not exactly a cut per se, but its an important step in an analysis which cannot be omitted. The results can be seen on Figures 39 and 40.

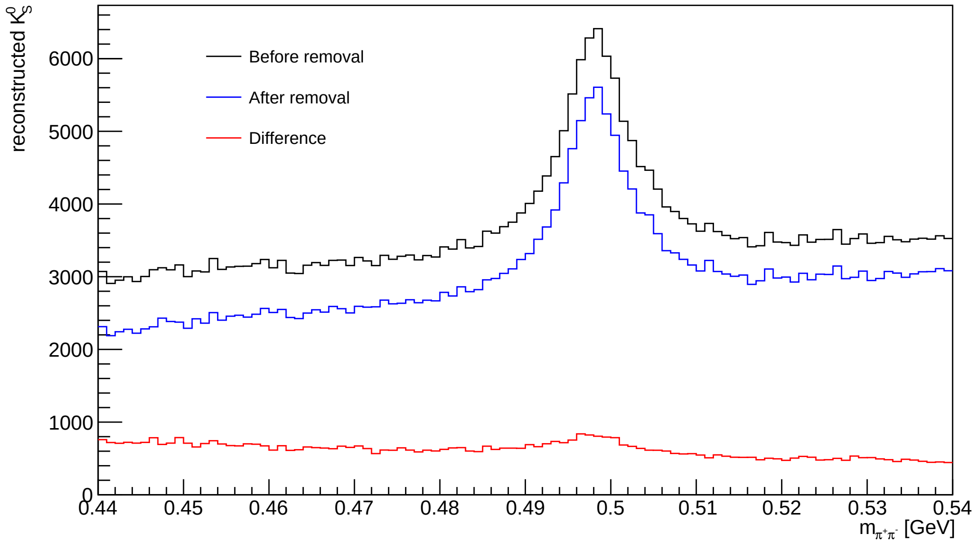

Figure 39: Difference after removing K^0_S reconstructions using same π^+/π^- entries

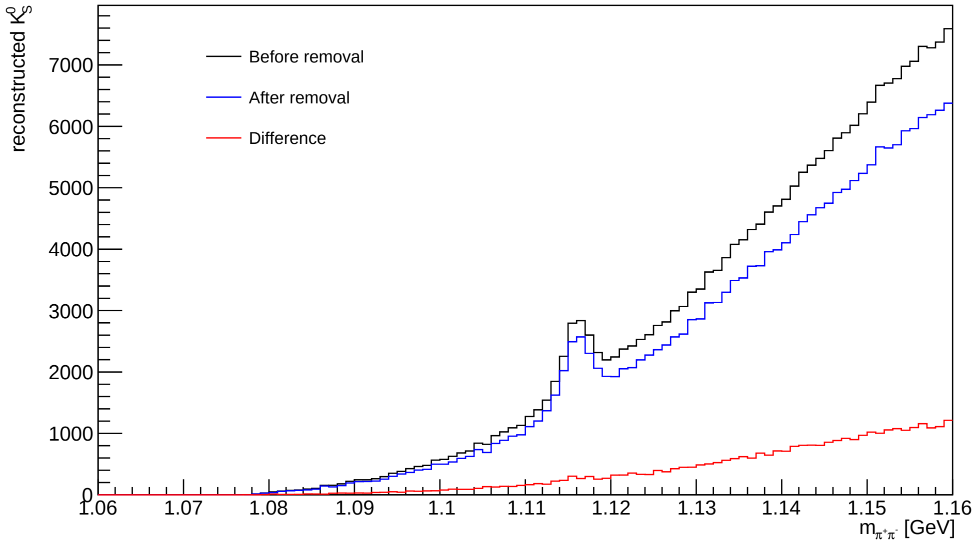

Figure 40: Difference after removing Λ^0 reconstructions using same p/π entries

As we can see, there are no huge visible peaks around K^0_S or Λ^0 masses in difference plot. Choosing the DCA of decay products as a sorting variable seems to be a good idea. However, given that the background is subtracted later on, leaving those duplicated entries actually might be a good idea, as there is a possibility of a small amount of signal getting cut away.

4 Possible improvements in event selection

Some cuts were tested and ultimately deemed not good enough or simply not working well with the current experimental setup. They are not the main part of the analysis, but they are shown nevertheless.

4.1 Particle Identification

Particle identification is based on measuring an energy loss of a particle and comparing it to Bethe-Bloch formula. Energy loss is estimated by its correlation with charge collected by endcap TPC pads. Due to changes in gas pressure, individual differences between pads and their actual lengths, it is impossible to properly average the particle energy loss due to ionisation fluctuations. As such, instead of the average energy loss, the most probable one is measured. It is achieved by removing part of clusters with the highest ionisation (typically upper 30%). The result of such measurement can be seen on Figure 41 - and while the measurements for that were taken under magnetic field of 0.25 T, the values under 0.5 T field remain largely the same, if not less scattered due to smaller transverse diffusion, which improves signal-to-noise ratio for every pad.

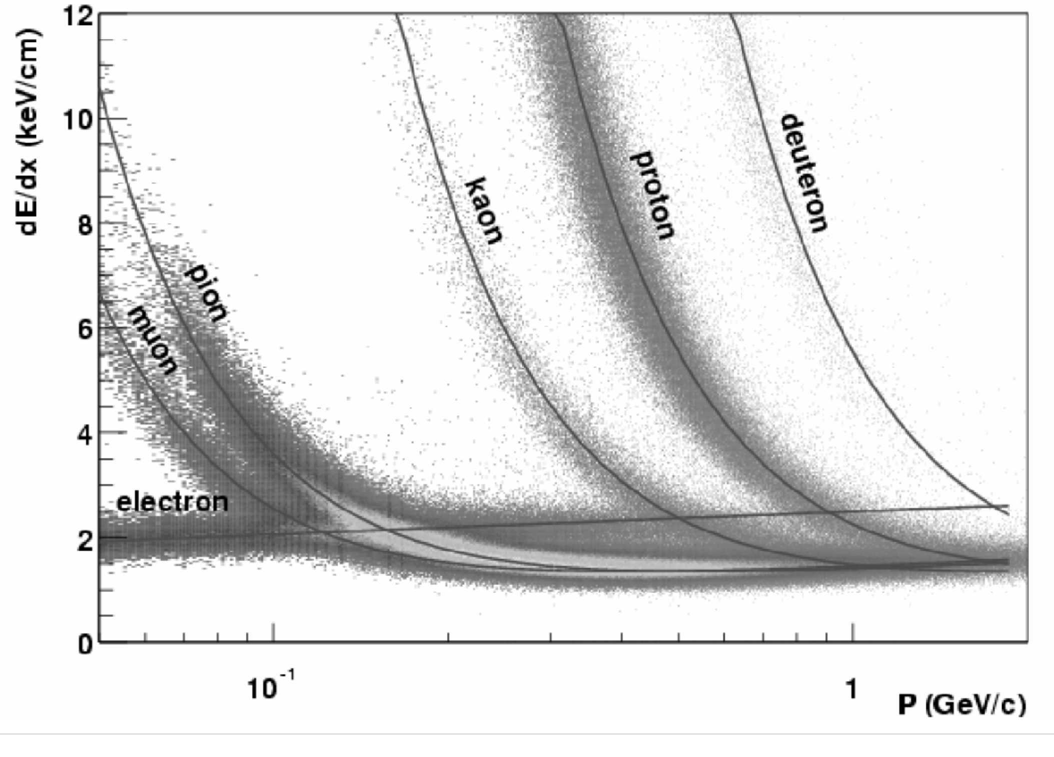

Figure 41: Energy loss distribution as a function of p_T. Magnetic field 0.25 T.

For easier data comparison, energy loss got from the measurement is transformed into gaussian-like distribution ($\mu = 0,\ \sigma = 1$) using formula below:

$$n_{\sigma_h} = \frac{\ln\left(\frac{dE}{dx}_h^{meas} / \frac{dE}{dx}_h^{teor}\right)}{\sigma_h^{teor}}$$

Theoretical values of $\frac{dE}{dx}$ and σ are calculated from TPC simulations. The "h" in the formula refers to the particle identified, as we currently have four possible "flavours" of identification: $h = \pi^{\pm}$, $K^{\pm}$, $p^{\pm}$ and $e^{\pm}$. The cuts tested in this analysis were as follows:

- For K^0_S:
  - Both pions $|n_{\sigma_\pi}| < 3$
- For Λ^0:
  - For pion $|n_{\sigma_\pi}| < 3$
  - For proton $|n_{\sigma_p}| < 3$

In my case, after all the cuts, the situation with all the particles taking part in K^0_S or Λ^0 reconstruction is shown on Figure 42. While according to [5] STAR was designed to be able to separate protons and pions with momenta up to 1.2 GeV/c, the problems however begin at around 0.4-0.5 GeV/c, where pions can be mistook for charged kaons. Protons are separated a bit better, and problems begins at 1 GeV/c, making the separation still not perfect, but due to the small amount of particles with such momentum - somewhat useful.

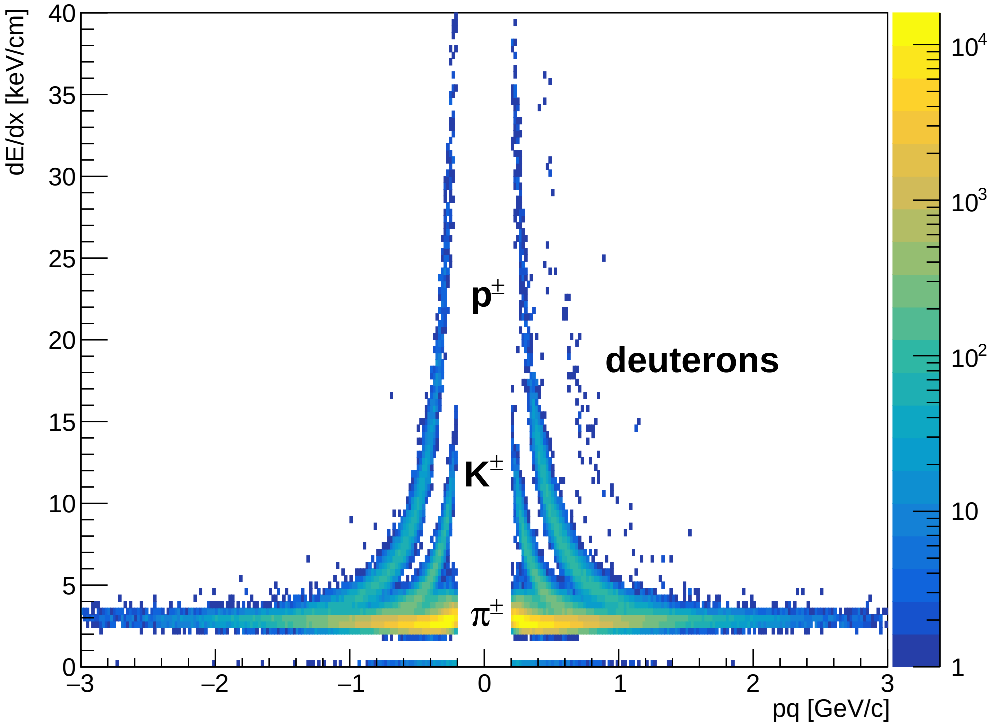

Figure 42: Energy loss distribution as a function of total momentum (sign of momentum means the sign of particle's charge).

Due to problems with differentiating charged kaons from pions, and statistical domination by pions, this cut is almost useless for purposes of K^0_S measurement, as it misidentifies more particles than it would be helpful. However, identifying the proton has tremendous influence on reducing the continuum background in Λ^0 measurements (as seen on Figure 43), which gives us hope in further research. While the reduction in Λ^0 number of detected particles is still happening, the effect on the background makes it worth considering.

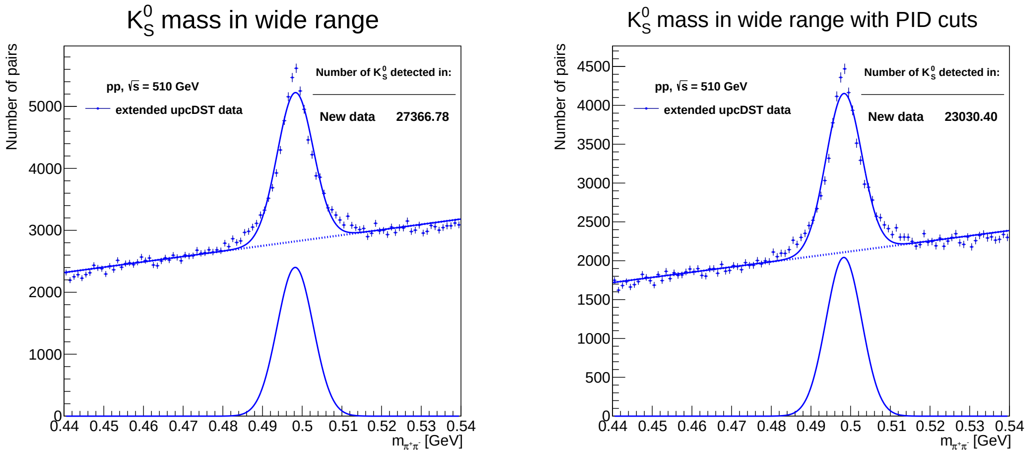

(a) K_S^0, without PID (b) K_S^0, with PID

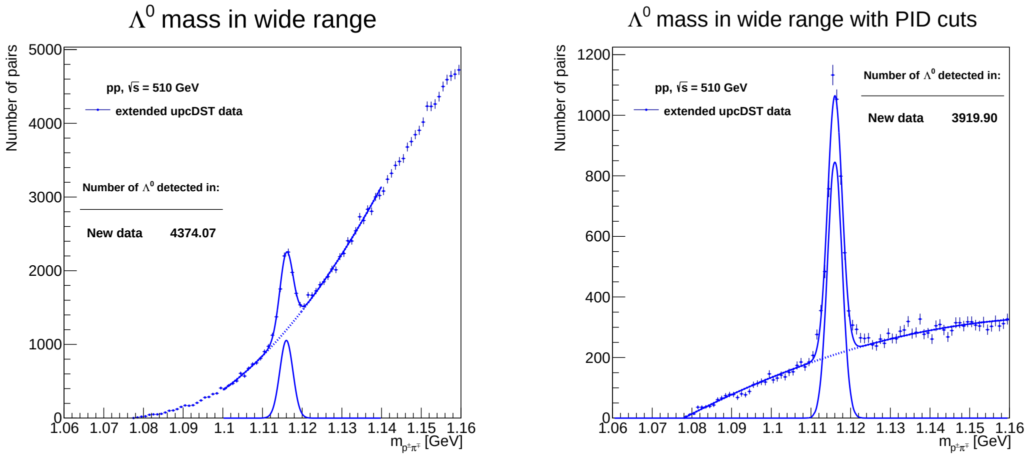

(c) Λ^0, without PID (d) Λ^0, with PID

Figure 43: Comparison of results with (right) and without (left) particle identification. Identifying a proton helps immensely, pions - not so much

4.2 TOF particle identification

The idea used here was taken from Rafał Sikora's PhD thesis [4]. We will walk through the process of its creation.

Having momentum of a particle from TPC, to calculate its mass, we would need its velocity. To calculate it, the measurement of time and distance needs to be taken. As we have parameterised the track, we know the distance the particle travelled - the timing information is the tricky part. We do not have the information about the exact time of particle creation, hence we cannot calculate the velocity and thus mass.

However, if we have two particles of the same mass, produced in a decay (such as $K_S^0 \to \pi^+\pi^-$ decay), we know their time of production is the same (denoted t_0 on Figure 44, while t_i and L_i are time of registering particle by ToF detector and the length of track, respectively).

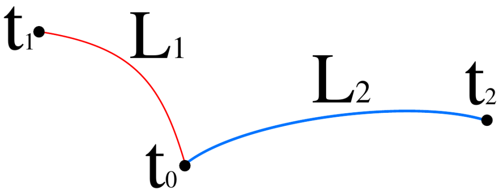

Figure 44: Scheme of two particles generated from one decay

Change of speed due to interaction with gas in TPC is negligible, so we can safely assume constant speed. We can express speed as a function of mass and othervariables, and get a set of two equations:

$$\begin{cases} \dfrac{L_1}{t_1 - t_0} = \dfrac{v_1\gamma_1 m_1 c^2}{\gamma_1 m_1 c^2} = \dfrac{p_1 c^2}{E_1} \\ \dfrac{L_2}{t_2 - t_0} = \dfrac{v_2\gamma_2 m_2 c^2}{\gamma_2 m_2 c^2} = \dfrac{p_2 c^2}{E_2} \end{cases}$$

After reorganising terms we can get them in a different form (here we also change the unit system to natural units, so $c = 1$):

$$\begin{cases} t_1 - t_0 = L_1\sqrt{1 + \dfrac{m_1^2}{p_1^2}} \\ t_2 - t_0 = L_2\sqrt{1 + \dfrac{m_2^2}{p_2^2}} \end{cases}$$

In this form, we can get rid of decay time t_0, and get it in one equation, where everything except masses is possible to measure:

$$t_1 - t_2 = L_1\sqrt{1 + \frac{m_1^2}{p_1^2}} - L_2\sqrt{1 + \frac{m_2^2}{p_2^2}}$$

If $m_1 = m_2 = m$, by proper term arrangement and squaring above equation twice, we can get a quadratic formula for m^2:

$$A(m^2)^2 + B(m^2) + C = 0$$

where A, B, C coefficients depend on measurable quantities.

Such idea would be useful for further reducing background for K_S^0 decay, and possibly, after changing $m_1 = m_2$ condition to something more akin to $m_1 = \frac{m_p}{m_\pi} m_2$, could be useful for Λ^0 decay. Unfortunately timing in the data was given in time units of internal ToF clock, which we did not find the proper documentation for. After talking with other members of STAR collaboration and some trying of my own, attempts were made, but they did not give back satisfactory results.

5 Results

The basic equation that allows us to connect the number of detected particles (N) with cross section for given reaction (σ) is as follows:

$$N = L\sigma\varepsilon \Leftrightarrow \sigma = \frac{N}{L\varepsilon}$$

where L is the integrated luminosity of the data-taking period, and ε is a coefficient depending on various factors changing the working number of events, such as detector efficiency and geometry, or prescaling factors.

With large enough yield, one can try to calculate differential cross section - how cross section depends on kinematic variables, such as η or p_T. This means dividing sample into subregions which allow to integrate differential cross section on different intervals and estimate the answer, which allows us to compare theory and results we got. An example ($N_{0-0.2}$ is number of K_S^0 with $0 < \eta < 0.2$):

$$\int_0^{0.2} \frac{d\sigma}{d\eta} d\eta = \sigma_{0-0.2} = \frac{N_{0-0.2}}{L \cdot \varepsilon_{0-0.2}}$$

For dividing sample into subregions, a 2D histograms are made (Figure 45) and then to each horizontal strip a gaussian signal+background function is fitted (Figure 46). For K_S^0 the linear background is enough, however Λ^0 needs a quadratic one.

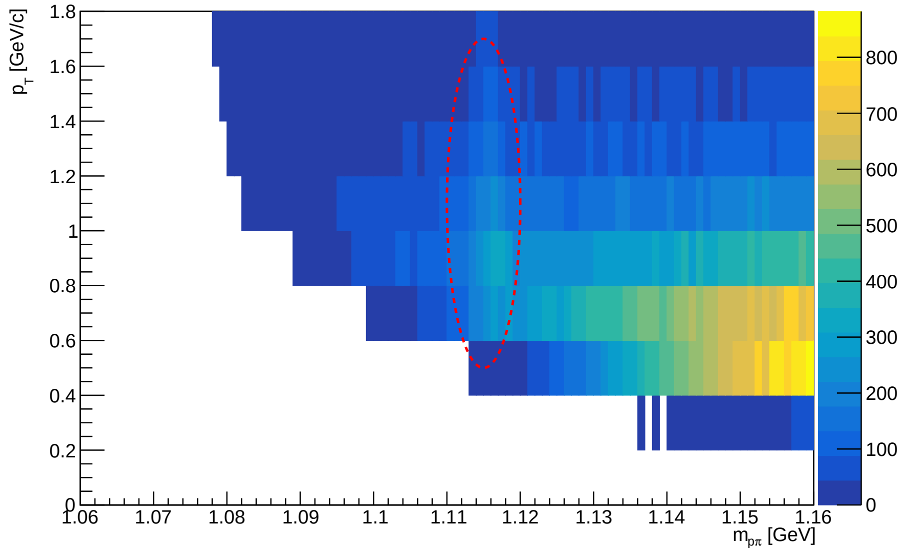

Figure 45: 2D histogram of Λ^0 particle, with respect to p_T. Red circle denotes the presence of Λ^0

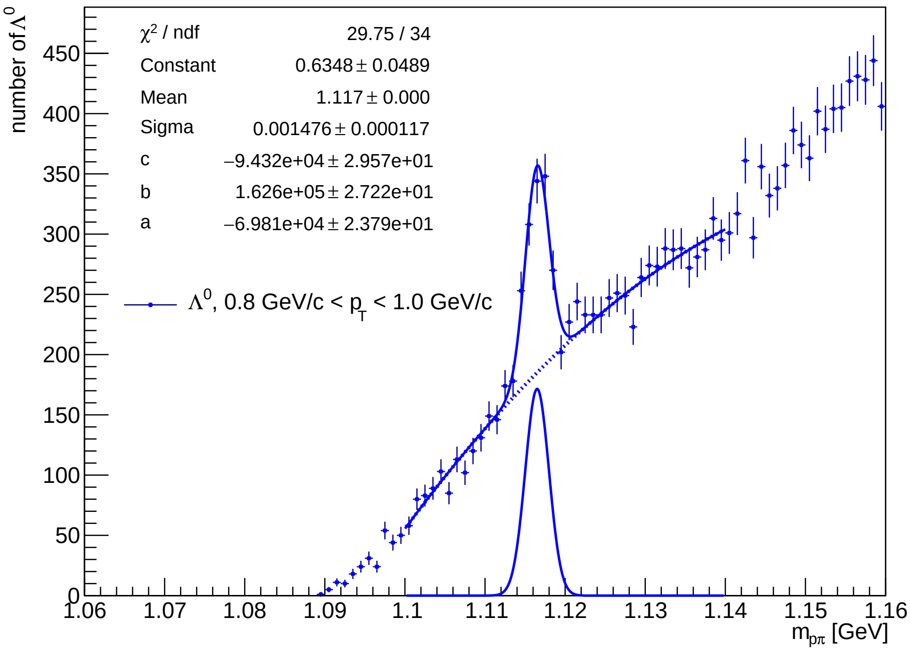

Figure 46: A slice of previous histogram, with all the fit parameters. Constant is linearly connected to the amount of detected Λ^0

Such plots were made as a function of yields of η and p_T in areas of significant signal (Figures 47 to 52). This means some bins of lower p_T values might be empty because of lack of data, and the "tails" continue further, but were impossible to model with current background noise. We can see this clearly on $\Lambda^0(p_T)$ plot above.

5.1 Differential yields

The results of this thesis are the plots 47 to 52. So far those are only differential yields, to use them for estimating differential cross section, a calculation of ε is needed. The histograms cut off regions with low amount of data, that is why they (especially those with regards to p_T) cut off at those values. Uncertainties visible on plots are taken from the fit of a gaussian peak. They were overlayed by results of PYTHIA8 simulation, normalised to the amount of detected particles on the given plot. PYTHIA8 simulation contains only geometrical acceptance of STAR detector without any reconstruction inefficiencies.
On histograms with regards to η we can see a drop in the middle, which is to be expected. We can also see slight asymmetries, which are assumed to exist due to detector effects (although drop for $\overline{\Lambda}^0$ seems huge, probably due to problems with fitting gaussian distribution).
On histograms with regards to p_T there exists a lack of data in low p_T area for Λ^0, which was caused by lack of reconstructed particles with such low transverse momenta, which is also correctly predicted by a simulation.

In general PYTHIA8 expectations describe data quite well. Some overestimation of the low p_T region by PYTHIA8 is expected since TPC reconstruction efficiency (assumed to be 100% in PYTHIA8 simulation) increases with p_T.

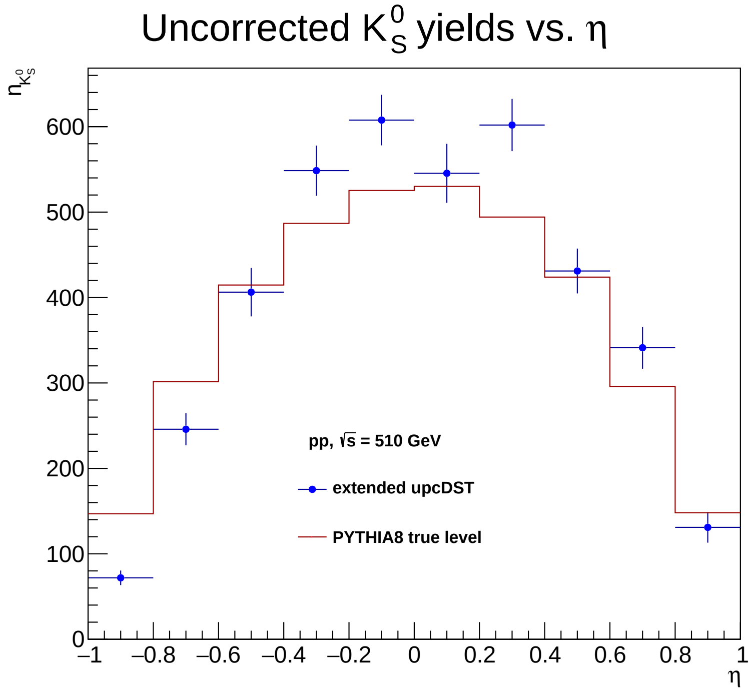

Figure 47: Differential yield of K_S^0 in regard to η.

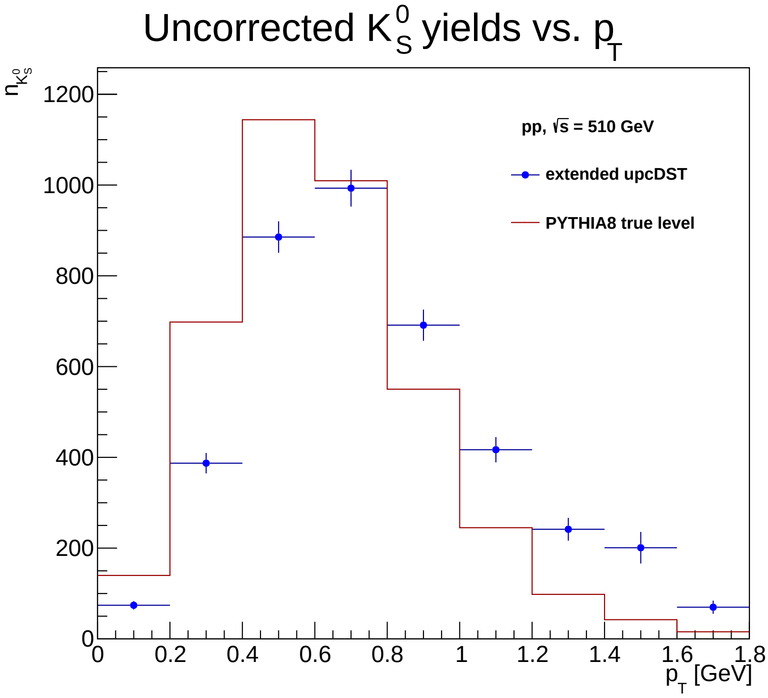

Figure 48: Differential yield of K_S^0 in regard to p_T.

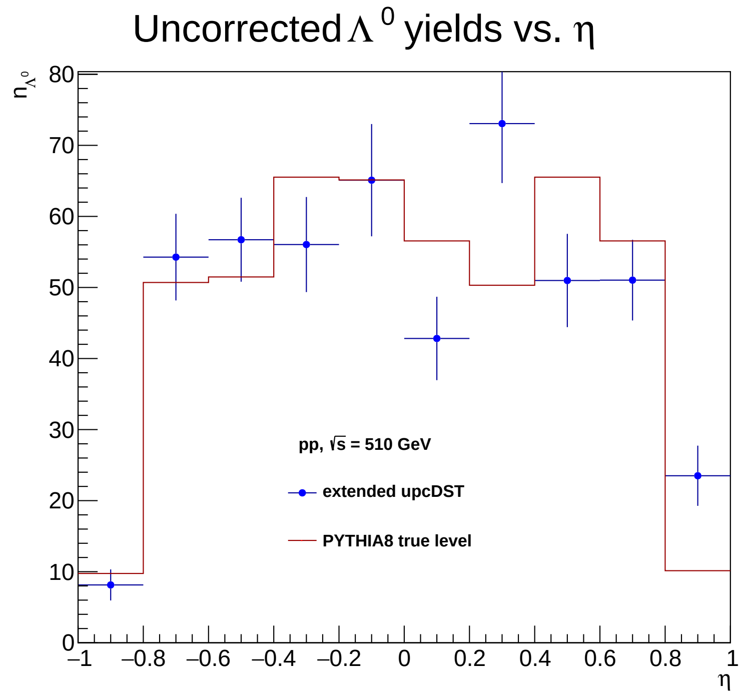

Figure 49: Differential yield of Λ^0 in regard to η.

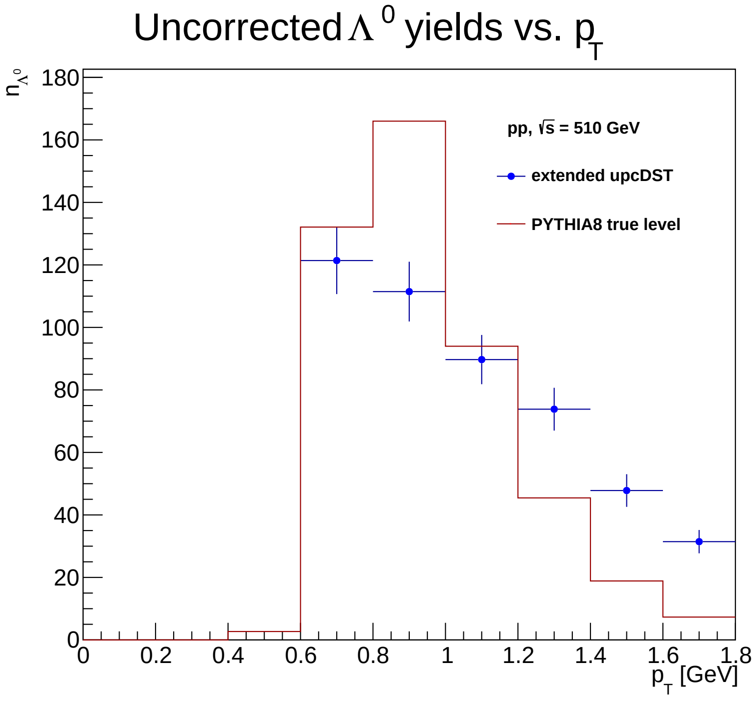

Figure 50: Differential yield of Λ^0 in regard to p_T.

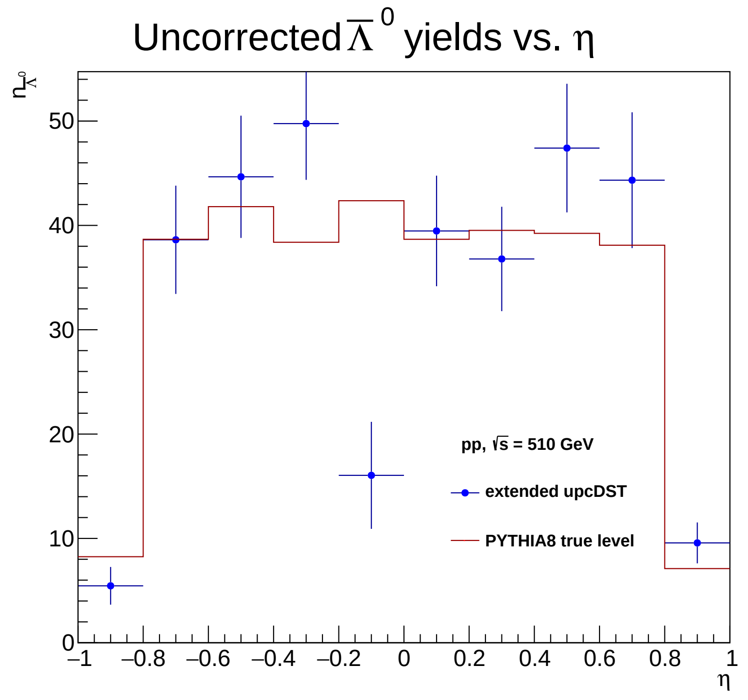

Figure 51: Differential yield of $\overline{\Lambda}^0$ in regard to η.

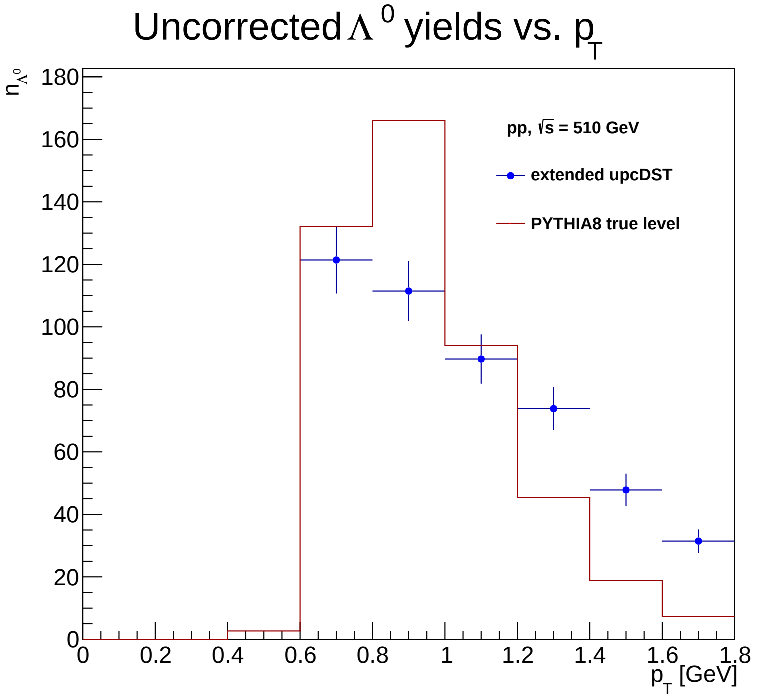

Figure 52: Differential yield of $\overline{\Lambda}^0$ in regard to p_T.

Reference

[1] Particle Data Group, M. Tanabashi et al. ,*Review of Particle Physics*, Phys. Rev. D 98, 030001 (2018)

[2] R. L. Workman *et al.* [Particle Data Group], PTEP **2022** (2022), 083C01 doi:10.1093/ptep/ptac097

[3] Tullio Regge, *Introduction to complex angular momentum*, Il Nuovo Cimento Series 10, Vol. 14, 1959, p. 951.

[4] R. Sikora, *Measurement of the diffractive central exclusive production in the STAR experiment at RHIC and the ATLAS experiment at LHC*, Ph.D. Thesis, AGH University of Science and Technology, CERN-THESIS-2020-235

[5] STAR Contributions to a NIM Volume Dedicated to the Detectors and the Accelerator at RHIC, https://www.star.bnl.gov/public/tpc/NimPapers/tpc/tpc_nim.pdf

[6] Proposal for a Large Area Time of Flight System for STAR, https://www.star.bnl.gov/public/tof/publications/TOF_20040524.pdf

[7] PYTHIA 8.3 manual, arXiv:2203.11601 [hep-ph]

[8] STAR Integrated Tracker Guide, https://www.star.bnl.gov/public/comp/meet/ITTFReviewSept2002/IttfDocumentation.pdf

[9] Feng Zhao, Strangeness Production and Strange V0 & Charged Hadron Correlation in Heavy-Ion Collisions https://github.com/ladamczy/STAR-Analysis/files/13540392/FengZhao_thesis.pdf

[10] Part of R. Debbe, "Coherent Diffraction off Au Nuclei Measured at RHIC with $\rho 0$ Mesons Detected with the STAR Setup." paper https://drupal.star.bnl.gov/STAR/files/userfiles/2729/file/TOFmatchingNote.pdf